CIRRELT

Centre interuniversitaire de recherche
sur les réseaux d'entreprise, la logistique et le transport

Interuniversity Research Centre
on Enterprise Networks, Logistics and Transportation

Goods Distribution with Electric Vehicles: Battery Degradation and Behaviour Modeling

Samuel Pelletier
Ola Jabali
Gilbert Laporte
Marco Veneroni

September 2015

CIRRELT-2015-43

Bureaux de Montréal :
Université de Montréal
Pavillon André-Aisenstadt
C.P. 6128, succursale Centre-ville
Montréal (Québec)
Canada H3C 3J7
Téléphone : 514 343-7575
Télécopie : 514 343-7121

Bureaux de Québec :
Université Laval
Pavillon Palasis-Prince
2325, de la Terrasse, bureau 2642
Québec (Québec)
Canada G1V 0A6
Téléphone : 418 656-2073
Télécopie : 418 656-2624

www.cirrelt.ca

Université Laval · McGill · Concordia · ÉTS · UQÀM · HEC Montréal · Polytechnique Montréal · Université de Montréal

Goods Distribution with Electric Vehicles: Battery Degradation and Behaviour Modeling

Samuel Pelletier[1], Ola Jabali[2,3,*], Gilbert Laporte[1,2], Marco Veneroni[4]

[1] Department of Management Sciences, HEC Montréal, 3000 chemin de la Côte-Sainte-Catherine, Montréal, Canada H3T 2A7

[2] Interuniversity Research Centre on Enterprise Networks, Logistics and Transportation (CIRRELT)

[3] Department of Logistics and Operations Management, HEC Montréal, 3000 Côte-Sainte-Catherine, Montréal, Canada H3T 2A7

[4] Dipartimento di Matematica "F. Casorati", Università degli Studi di Pavia, Via Ferrata 1, 27100 Pavia, Italy

Abstract. The use of electric vehicles for goods distribution opens up a wide range of research problems. Battery electric vehicles (BEVs) operate on batteries that have a limited life, as well as specific charging and discharging patterns which need to be considered in the context of their use for goods distribution. While many transportation problems associated with the integration of freight electric vehicles in distribution management problems have been investigated, there is room for further research on specifically how to model battery degradation and behaviour in such problems. The aim of this paper is to provide tractable models for transportation scientists that will allow predicting the lifetime degradation and instantaneous charging and discharging behaviour of BEV batteries.

Keywords: Electric vehicles, battery degradation, battery behaviour, battery modeling, green transportation.

Acknowledgements. This research was partly supported by the Natural Sciences and Engineering Research Council of Canada (NSERC) under grants 463834-2014, 436014-2013 and 2015-06189. This support is gratefully acknowledged. Thanks are also due to Olivier Tremblay for sharing his knowledge of battery modeling with us.

Results and views expressed in this publication are the sole responsibility of the authors and do not necessarily reflect those of CIRRELT.

Les résultats et opinions contenus dans cette publication ne reflètent pas nécessairement la position du CIRRELT et n'engagent pas sa responsabilité.

---

* Corresponding author: Ola.Jabali@cirrelt.ca

Dépôt légal – Bibliothèque et Archives nationales du Québec
Bibliothèque et Archives Canada, 2015

© Pelletier, Jabali, Laporte, Veneroni and CIRRELT, 2015

1. Introduction

Green transportation and city logistics seek ways of reducing transportation externalities in urban settings, such as forbidding or restricting the use of heavy vehicles in city centers (see, e.g., Bektaş and Laporte (2011); Demir et al. (2014); Gonzalez-Feliu et al. (2014); Psaraftis (2015)). The research carried out in these fields focuses on the design of distribution policies that will help decrease the environmental impact of goods distribution. An important research area lies in the development of models that can accurately predict exhaust emissions of conventional vehicles (e.g., Demir et al. (2011); Kamarianakis et al. (2011)). In addition, in recent years we have witnessed an increased interest in topics such as vehicle fleet composition in green logistics (e.g., Stasko and Gao (2012); Kopfer and Kopfer (2013); Kopfer et al. (2014); Koç et al. (2014); Goeke and Schneider (2015); Sassi et al. (2015)). In the same vein, increasing attention is being paid to the use of battery electric vehicles (BEVs) as a means to yield green distribution practices (Pelletier et al. (2015)).

Beyond the uncertainties surrounding the environmental impacts of freight electric vehicles, there exist performance and financial issues associated with their integration into distribution schemes. Although offering the advantage of much lower energy and maintenance costs, these vehicles typically have autonomy and payload limitations, and involve much larger initial investments in comparison with internal combustion engine vehicles. A common denominator to these financial and technical limitations is the vehicle's battery. The most common kind of batteries used in modern passenger and freight BEVs are lithium-ion batteries (den Boer et al. (2013)), which in addition to being costly and restricting the payload and range of freight BEVs, have a limited lifespan and specific charging and discharging behaviours.

1.1 Motivation for battery degradation modeling

In most cases where BEVs are used for goods distribution, these are mainly charged at depots overnight and do not use public charging stations outside the drivers' breaks (Nesterova et al. (2013), Naberezhnykh et al. (2012), Taefi et al. (2015)). This can be explained by the need to use the drivers' time efficiently and by security concerns (Naberezhnykh et al. (2012)). Charging automotive lithium-ion batteries can take hours depending on the equipment used and on the capacity of the battery (US DOE (2012)), making fast charging infrastructures necessary for recharging during delivery routes; these, however, are almost inexistent in most countries (IEA and EVI (2013)). En route recharging facilities are only useful in contexts

where BEV routes are highly constrained by the battery capacity. Since one of the effects of lithium-ion battery degradation is a loss of battery capacity and hence a decrease in the vehicle's achievable range (Barré et al. (2013)), and since such autonomy declines have been reported in actual freight BEV deployments (Taefi et al. (2015)), long term operational flexibility can be preserved by taking steps to ensure that the battery is not excessively aged when this can be avoided.

Lithium-ion battery packs for BEVs are a major cost component of these vehicles (Electrification Coalition (2013)). The cost of BEV lithium-ion battery packs per kWh were up to $800 in 2012 (Cluzel and Douglas (2012), Dulcep et al. (2011)) and should remain above $300/kWh in the next ten years (Gerssen-Gondelach and Faaij (2012)). However, it has recently been suggested that they have been decreasing faster than predicted and could already be about $400/kWh (Nykvist and Nilsson (2015)). Nevertheless, considering that the lithium-ion battery packs in battery electric trucks can have approximate energy capacities of 100 kWh (e.g., Smith Electric Vehicles (2015); Electric Vehicles International (2015)) and sometimes much more (e.g., Balqon Corporation (2013)), the battery still represents a significant portion of the vehicle's cost. Several factors regarding storage and operating conditions can influence the lifespan of these batteries (Barré et al. (2013)). Moreover, having to replace the battery in electric delivery trucks over the course of their lifetime has been shown to significantly decrease their attractiveness (Davis and Figliozzi (2013); Feng and Figliozzi (2013); Lee et al. (2013)). It therefore also seems logical from a cost perspective to try to incorporate certain battery health considerations into distribution schemes with BEVs.

1.2 Motivation for battery behaviour modeling

Several recent studies have successfully handled the routing issues associated with the integration of BEVs in distribution management problems, such as limited range and payload, and the possibility of recharging en route at stations or at the depot. Regarding battery modeling, most studies have treated the battery as having a fixed energy capacity. Such papers have modeled the charging process either as a fixed charging time penalty (Afroditi et al. (2014), Preis et al. (2014), Conrad and Figliozzi (2011)), as an energy recharging rate per unit of time (e.g., Lebeau et al. (2015), Hiermann et al. (2014), Goeke and Schneider (2015), Schneider et al. (2014), Bruglieri et al. (2015), Felipe et al. (2014)), or with piecewise linear approximations based on experimental data (Zündorf (2014)). During discharging, the energy capacity of the battery is either assumed to decline linearly according to the distance traveled (e.g., Hiermann et al. (2014), Schneider et al. (2014), Bruglieri et al. (2015),

Felipe et al. (2014), Sassi et al. (2015)), or by an amount determined according to an energy consumption model based on road forces acting on the vehicle (e.g., Lebeau et al. (2015), Goeke and Schneider (2015), Preis et al. (2014)).

It is clear that several routing problems associated with the use of freight BEVs have been solved, thus demonstrating that operations research can help to successfully integrate these vehicles into distribution operations by modeling and solving relevant problems (e.g., optimal paths, fleet size and mix, vehicle routing) which take into account the specific characteristics of these vehicles (Pelletier et al. (2015)). However, we believe that there is still room for further development regarding how to model the battery's discharging and recharging processes in a tractable way, which is still capable of taking certain fundamental battery behaviour characteristics into account.

For example, a battery's capacity should ideally be treated as a measure of electrical charge rather than energy (Sauer (2009)). The battery's state of charge (SOC) should therefore refer to the current proportion of electrical charge inside the battery with respect to the maximum possible charge it can hold (Bergveld (2001)), as opposed to the current amount of energy inside the battery with respect to a maximum energy capacity, as is typically the case in transporation planning problems. As a result, the instantaneous variation of the battery's SOC can be defined as the electrical current coming in or out of the battery divided by its maximum capacity (Moura et al. (2011)), since current is a measure of electrical charge per unit of time. Furthermore, the power output of a battery corresponds to the product of its terminal voltage and current (Khajepour et al. (2014)), both of which are subject to variations while discharging, according to the power profile associated with the driving cycle (Campbell (2011)). Even when assuming that a BEV travels at constant speed and hence requires a constant battery power output, the battery's terminal voltage (as it partly depends on the SOC) would decrease while discharging and its current would need to increase in order to maintain the required power output (Sauer (2009)). The battery's SOC variation with time therefore depends on the electrical current profile associated with the driving cycle.

Moreover, there exists a difference between available and maximum capacity. The latter varies with temperature and will fade over the battery's life, but the former also decreases when the battery is discharged with larger currents (Lam (2011)). This is because in order to avoid certain degradation mechanisms, the discharging process must be stopped when the battery's terminal voltage decreases to a certain cut-off value (Wenzl (2009)). Since the battery's terminal voltage can be modeled as a function of both the current and the SOC (Larminie and Lowry (2003)), the end of the discharging process can occur at several SOC values due to different voltage drops resulting from different discharging currents (Chen and

Rincón-Mora (2006)). Thus, if the SOC is defined with respect to the maximum capacity under a reference temperature, the end of discharge will be reached at a SOC higher than 0%, since larger currents cause larger voltage drops, and hence the maximum capacity will only be fully delivered under an infinitely small discharging current (Lam (2011)). This also implies that a battery discharged with a large current which has reached its cut-off voltage could actually be further discharged if the current was reduced (Bergveld (2001)). In the same vein, the available energy during a specific discharging cycle will also depend on the terminal voltage and on the current profile required to provide the power output, with the total delivered energy obtained by integrating their product over discharge time (Khajepour et al. (2014)).

There also exist some interesting battery empirical degradation models that consider the battery's charge throughput (i.e., the amount of electrical charge coming in and out of the battery) as well as the charging and discharging current to estimate the battery's capacity fade, both of which require the knowledge of the battery's electrical current. In addition, the battery in an electric vehicle is often charged with a constant current-constant voltage (CC-CV) scheme (Liu (2013)). The charging current is held constant during the first phase (CC) and hence the SOC increases linearly with time until the battery's terminal voltage increases to a specific maximum value. Allowing the battery to reach a higher voltage will cause overcharging degradation to occur (Lam (2011)). Therefore, the terminal voltage is then held constant at its maximum value in the second phase (CV), thus causing the current to decrease exponentially and the SOC to increase concavely (Marra et al. (2012)). Another alternative is to charge the battery with a constant power-constant voltage (CP-CV) scheme. The CC phase is then replaced by a CP phase during which the current decreases with time while the terminal voltage increases to maintain the constant charging power (Liu (2013)). In both cases, models linking the battery's terminal voltage to the charging current and SOC must be employed to represent the charging process more accurately.

1.3 Aim and organization of this paper

For the reasons stated above, in the context of transportation planning problems with BEVs, there is a need for more elaborate modeling approaches to represent the battery's degradation over its lifetime, as well as to account for its instantaneous charging and discharging behaviours. The objective of this paper is to provide helpful information to understand these features, as well as tractable models to predict their behaviour. These contributions should prove useful to the growing community of transportation scientists involved in the develop-

ment of models and algorithms for goods distribution by BEVs, several of which partly rely explicitly on battery degradation and instantaneous behaviour functions. With this goal in mind, Section 2 provides a brief description of lithium-ion batteries, their current status and expected future projections. Section 3 describes the mechanisms that cause degradation to occur and lists a few interesting aging models that allow the prediction of capacity fading over battery lifetime. Section 4 investigates how the fundamental instantaneous charging and discharging behaviour of the battery can be taken into account by appropriately aggregating a number of existing models and principles. Finally, conclusions and insights are drawn in Section 5. Appendix A contains a glossary of the technical terms used in this study.

2. Lithium-ion batteries

Currently available options for batteries in electric vehicles are lead-acid batteries, nickel-metal hydride batteries, sodium-nickel-chloride batteries (also called ZEBRA batteries), and lithium-ion batteries (Yong et al. (2015)). Since lithium-ion batteries have a high specific energy, high specific power, good lifespan attributes and low memory effect (Lukic et al. (2008)), they are currently the most commonly used battery technology in modern BEVs. Lithium-ion batteries are also the leading option for plug-in hybrid electric vehicles (PHEVs), but nickel-metal-hydride batteries are still used in non-plug-in hybrid electric vehicles (HEVs) which do not require such a high specific energy (Cluzel and Douglas (2012)). Lead-acid batteries have an even lower specific energy and are thus limited to low performance BEVs and micro-HEVs (Gerssen-Gondelach and Faaij (2012)). ZEBRA batteries have a good specific energy and have been used in earlier freight BEVs (Nesterova et al. (2013)), but their low specific power and very high operating temperature are significant drawbacks compared to lithium-ion batteries (Gerssen-Gondelach and Faaij (2012)).

2.1 How lithium-ion batteries function

The purpose of any rechargeable battery is essentially to employ reduction and oxidation (redox) reactions in order to store energy during charging, and subsequently use it to accomplish work during discharging (Moura (2011)). Automotive lithium-ion batteries are made of many electrochemical lithium-ion cells which are first assembled into modules and then into a battery pack to reach the desired capacity and voltage (Cluzel and Douglas (2012)). The same lithium-ion technology is behind the batteries of passenger and freight BEVs, the latter using packs with more cells or larger cells (den Boer et al. (2013), Cluzel and Douglas

(2012)). In each cell, lithium ions are displaced between two intercalation electrodes during charging and discharging while electrons flow through an external circuit. This process is summarized in Figure 1.

The electrodes are the components looking to react with each other (i.e., provoking the redox reactions), while the electrolyte allows ions to move back and forth between these within the battery (Tarascon and Armand (2001)). The electrolyte also contains a separator to ensure that the electrodes do not come into direct contact (to prevent a short circuit) while still allowing the lithium ions to traverse its pores (Cluzel and Douglas (2012)). While discharging, the electrons and lithium cations (i.e., positive ions) simultaneously flow from the negative electrode (i.e., the anode) to the positive one (i.e., the cathode), with the electrons traversing an external electric circuit and the ions traversing the electrolyte solution; the process is reversed when the battery is charged (Cluzel and Douglas (2012)). The oxidation reaction (i.e., the loss of electrons) therefore occurs at the anode and the reduction reaction (i.e., a gain of electrons) occurs at the cathode when the battery is being discharged. The electrolyte is essential for these reactions to occur (i.e., for electrical current to be generated) since it allows positive lithium ions to move from one electrode to the other. This neutralizes the charges that form during the loss and gain of electrons at each side and thus completes the chemical reaction (Aravindan et al. (2011)). Current collectors are also connected to each electrode via a binder in order to link the active materials of the cell to the external circuit (Lam (2011)).

In summary, the idea is to force lithium ions into a disfavored higher energy state at the anode during charging (by transforming the provided electrical energy into chemical energy), and only allow them to return to a preferred lower energy state at the cathode during discharging when an external electrical circuit is connected and the discharging redox reactions can occur (by transforming the stored chemical energy into electrical energy), thus taking advantage of the movement of electrons in the process to accomplish work.

2.2 Performance assessment

There exist several different kinds of lithium-ion batteries, varying according to the materials used in their cells and ultimately presenting pros and cons regarding attributes such as energy, power, safety, lifespan and cost (Dinger et al. (2010)). In currently available lithium-ion batteries, the cathode typically consists of some lithium metal oxide (e.g., Figure 1 depicts a lithium cobalt oxide cathode) or lithium iron phosphate compound, while graphite is commonly used for the anode; the electrolyte is often a lithium salt in an organic solvent

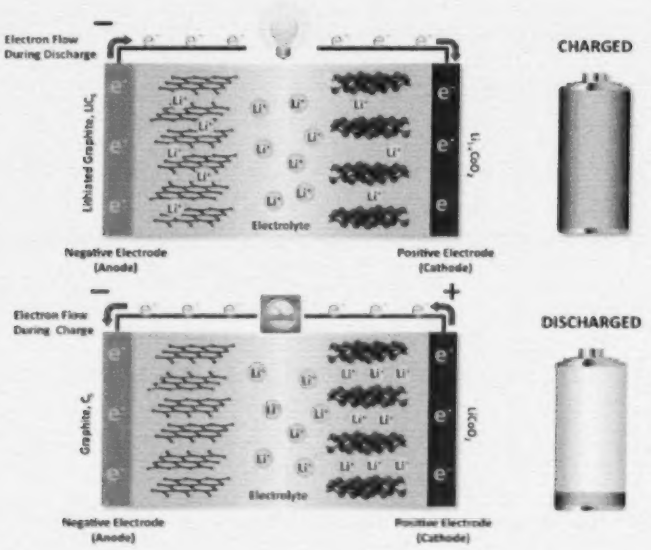

Figure 1: Schematic representation of lithium-ion battery function
(Source : Thackeray et al. (2012))

(Cluzel and Douglas (2012)). Cathodes can also consist of a combination of different chemical compounds for performance and cost reasons (Thackeray et al. (2012)).

Electric vehicles in distribution schemes typically involve the delivery of goods to customers, and thus the use of freight BEVs such as trucks. Several electric truck manufacturers have opted for some form of lithium iron phosphate compound for the cathode in their vehicles' lithium-ion battery (e.g, Boulder Electric Vehicle (2015), Balqon Corporation (2015)). Lithium iron phosphate batteries typically provide good safety and lifespan attributes compared with other options, at the expense of a somewhat lower specific energy (Dinger et al. (2010)). Some electric truck manufacturers have attempted to increase the performance of their vehicles by adding other metals such as magnesium to the conventional LiFePO4 cathode (e.g., Electric Vehicles International (2015)), or by using nanoscale materials (e.g., A123 (2015)). Much research is still conducted to develop better component materials and combinations aimed at improving the performance of lithium-ion batteries (Thackeray et al. (2012)).

Battery weight is a key consideration for goods distribution with BEVs since it forces trade-offs to be made between payload and range. As previously mentioned, the amount of energy that a battery can deliver varies according to the load conditions, and hence so does its specific energy (Larminie and Lowry (2003)). Nevertheless, approximate values for

energy and power contents per unit of mass can be helpful for comparison purposes with other fuel types. Current automotive lithium-ion cells have a specific energy ranging from 100 to 180 Wh/kg, depending on the materials used (Cluzel and Douglas (2012)). While the specific energy of lithium-ion cells is expected to increase in the future, the development of technologies with lithium metal anodes such as lithium-sulfur (Li-S) and lithium-air (Li-air) batteries should allow reaching values above 500 Wh/kg (Bruce et al. (2012)). Zinc-air (Zn-air) batteries are another option under development which could improve specific energy (Yong et al. (2015)). Furthermore, the final battery pack can have a specific energy up to 40% lower than the cells due to additional packaging components, thus estimated to be between 80 and 120 Wh/kg for BEVs in 2010 (Dinger et al. (2010)). Projections made in 2012 from Gerssen-Gondelach and Faaij (2012) for BEV lithium-ion battery packs and other potential BEV battery types (Li-S, Li-air and Zn-air) are provided in Table 1. Note that these projections do not imply that all issues associated with new battery technologies (e.g., safety and cycle life for Li-S; specific power and efficiency for Zn-air; safety, cycle life, and specific power for Li-air) will necessarily be resolved by 2025; lithium-air batteries in particular are much less developed and thus considered to be a longer term solution (Gerssen-Gondelach and Faaij (2012)).

While specific power is considered to be an issue associated with other potential battery technologies for BEVs of the future (Gerssen-Gondelach and Faaij (2012)), this is not so much the case for lithium-ion batteries since these can already offer similar power capabilities as internal combustion engines (Dinger et al. (2010)). The specific power of current lithium-ion cells can take many values according to design trade-offs between specific power and specific energy (e.g., PHEVs require significant power from smaller batteries), thus ranging from roughly 200 W/kg to 2000 W/kg (Cluzel and Douglas (2012)). Lithium-ion battery packs in current BEVs should provide approximately 400 W/kg, with 500 W/kg expected by 2025 (Gerssen-Gondelach and Faaij (2012)).

Diesel fuel, on the other hand, has a specific energy of approximately 12,500 Wh/kg (ACEA (2013)). Even taking into account the fuel tank's weight in conventional vehicles and the fact that battery electric trucks can be three to four times more efficient than similar diesel trucks from a tank-to-wheel perspective (Gallo and Tomić (2013), Lee et al. (2013)), the difference in energy actually used to turn the wheels per kilogram of the on-board energy storage system remains very significant. Although the range of freight BEVs may become less constraining in the future with the development of battery technologies, it remains that current ranges typically vary from 100 to 200 kilometers for freight BEVs (Nesterova et al. (2013), AustriaTech (2014)), and can temporarily decrease due to several external factors

such as heavy loads, upward slopes, high speeds, and quick acceleration (US DOE (2012)).

Table 1: Projections for current and other promising BEV battery technologies (Source: Gerssen-Gondelach and Faaij (2012))

		Li-ion	Li-S	Zn-air	Li-air
Specific energy (Wh/kg)	2015	150	Not applicable	Not applicable	Not applicable
	2025	200	400	250	500
	Beyond 2025	250	500	350	1000
Specific power (W/kg)	2015	400	Not applicable	Not applicable	Not applicable
	2025	500	300	Unknown	Unknown
	Beyond 2025	500	400	Unknown	Unknown
Cost ($/kWh)	2015	400-600	Not applicable	Not applicable	Not applicable
	2025	300-400	Highly uncertain	Highly uncertain	Highly uncertain
	Beyond 2025	250-300	250-500	100-300	350-700

3. Lithium-ion battery degradation

The health of lithium-ion batteries can be negatively influenced by the way they are used and stored, the former corresponding to cycle aging and the latter to calendar aging (Barré et al. (2013)). The two main consequences of battery degradation in electric vehicles are capacity fade, which reduces the vehicle's achievable range, and impedance raise, which reduces the battery's available power output (Barré et al. (2013)). The end of life of the battery in BEVs is usually considered to occur when its available capacity or maximum power under reference conditions has decreased by 20% of its original value, although the loss of capacity is typically the determining factor given that the initial power capabilities of the battery are superior to what the vehicle requires (Lam (2011)). Current lithium-ion cells for BEVs usually have a five to ten year life according to the cell chemistry and the way they are managed (Cluzel and Douglas (2012)), and should be able to provide 1,000 to 2,000 cycles when cycled with large SOC variations, with 4,000 cycles expected in the near future (den Boer et al. (2013)).

The objective of this section is twofold: to investigate what causes the performance of lithium-ion batteries to fade over their lifespan, and to determine whether such aging

can be modeled in a tractable way. In order to fulfil this objective, Section 3.1 describes the primary mechanisms causing degradation to occur in lithium-ion batteries, as well as operating conditions which tend to enhance the effect of such mechanisms. Section 3.2 then presents a few practical models which allow predicting the degradation resulting from certain stress factors over the course of a battery's lifetime.

3.1 Degradation mechanisms and aggravating factors

A significant portion of the deterioration of current lithium-ion cells with a graphite anode stems from chemical side reactions that occur between the anode and the electrolyte at their interface, resulting in the formation of a solid electrolyte interphase (SEI) on the anode's surface and the simultaneous consumption of lithium ions during the reaction, thus causing power and capacity fade respectively (Vetter et al. (2005), Tan et al. (2013), Zheng et al. (2015a)). In the battery's first cycles, the formation of the SEI on the anode is desirable since it prevents excessive electrolyte decomposition and anode corrosion in the future while still allowing lithium ions to traverse it (Vetter et al. (2005)). However, the SEI film slowly continues to grow and rearrange itself as well as to consume lithium over the course of the battery's life, and the battery's performance therefore continues to deteriorate (Vetter et al. (2005), Tan et al. (2013), Zheng et al. (2015a)). Solid surface layers may also form at the interface of the cathode and the electrolyte (Vetter et al. (2005)), although they are much thinner than those formed on the anode (Hausbrand et al. (2015)). The reactions occurring at the interfaces of the electrodes and the electrolyte can also reduce the electrolyte's capability to allow lithium ions to flow through it as well as release unwanted gaseous side products (Moura (2011)). In addition the electrodes can experience structural and chemical deterioration over the battery's lifespan (Moura (2011)). Overviews of anode and cathode aging mechanisms are provided in Table 2 and Figure 2, respectively.

There exist certain operating and storage conditions that tend to enhance these degradation mechanisms. Keeping the cell at a high SOC or in high temperatures as well as using high charging or discharging rates can accelerate degradation resulting from electrolyte decomposition and the SEI development on the graphite anode (Vetter et al. (2005), Barré et al. (2013), Zheng et al. (2015c), Zheng et al. (2015b)). Larger SOC variations during cycling may accelerate power fade via the growth of the SEI and possible damage to the cathode materials (Belt et al. (2003)). A larger depth of discharge (DOD, i.e., cycling SOC swing) can also cause contact losses between certain components on the anode side due to volume variations of anode materials during cycling (Vetter et al. (2005)).

Table 2: Overview of lithium-ion battery anode aging mechanisms (Source : Vetter et al. (2005))

Cause	Effect	Leads to	Reduced by	Enhanced by
Electrolyte decomposition (→ SEI) (Continuous side reaction at low rate)	Loss of lithium Impedance rise	Capacity fade Power fade	Stable SEI (additives) Rate decreases with time	High temperatures High SOC
Solvent co-intercalation, gas evolution and subsequent cracking formation in particles	Loss of active material (graphite exfoliation) Loss of lithium	Capacity fade	Stable SEI (additives) Carbon pre-treatment	Overcharge
Decrease of accessible surface area due to continuous SEI growth	Impedance rise	Power fade	Stable SEI (additives)	High temperatures High SOC
Changes in porosity due to volume changes, SEI formation and growth	Impedance rise Overpotentials	Power fade	External pressure Stable SEI (additives)	High cycling rate High SOC
Contact loss of active material particles due to volume changes during cycling	Loss of active material	Capacity fade	External pressure	High cycling rate High DOD
Decomposition of binder	Loss of lithium Loss of mechanical stability	Capacity fade	Proper binder choice	High SOC High temperatures
Current collector corrosion	Overpotentials Impedance rise Inhomogeneous distribution of current and potential	Power fade Enhances other aging mechanisms	Current collector pre-treatment	Overdischarge Low SOC
Metallic lithium plating and subsequent electrolyte decomposition by metallic lithium	Loss of lithium (loss of electrolyte)	Capacity fade (power fade)	Narrow potential window	Low temperature High cycling rate Poor cell balance Geometric misfits

Overcharging the battery (i.e., allowings its terminal voltage to exceed the specified cut-off value) can result in the formation of dendrite on the anode (i.e., metallic lithium deposits), thus wasting more cyclable lithium (Ouyang et al. (2015)). If continuously expanded, the dendrite can even puncture the separator and result in severe overheating (Moura (2011)). Lithium plating on the anode can also develop as a result of low temperatures (Vetter et al. (2005), Barré et al. (2013)) and high charging rates (Trippe et al. (2014)). A loss of active cathode materials can also occur when the battery is overcharged (Lam (2011)).

Graphite anodes can be subject to mechanical degradation (e.g., cracks and fissures) when using high charging rates in high SOC levels (Agubra and Fergus (2013)). Furthermore, certain conditions (e.g., high temperatures, low and high SOC levels) can result in the dissolution of the active materials of certain cathodes into the electrolyte as ions which can eventually end up growing the SEI film on the anode (Vetter et al. (2005), Amine et al.

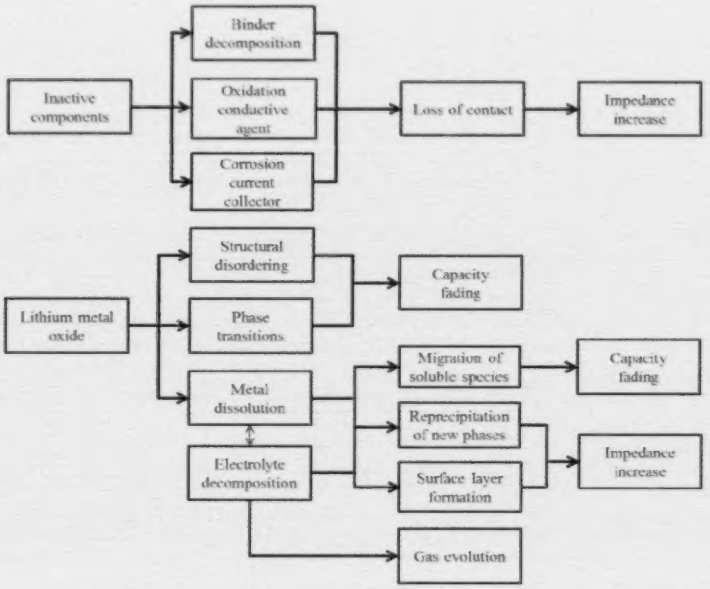

Figure 2: Overview of lithium-ion battery cathode aging mechanisms (Source : Wohlfahrt-Mehrens et al. (2004))

(2005)).

Current collectors on the electrodes may also contribute to certain degradation mechanisms; for example, there could be dissolution of the anode's copper current collector when the battery is discharged to low voltage levels (i.e., near or beyond the cut-off voltage), subsequently forming dendrites on the anode which may also eventually puncture the separator (Arora et al. (1998)). Current collector corrosion resulting from excessively low voltage levels can also lead to diminished contact with the anode's materials (Vetter et al. (2005)).

In summary, lithium-ion battery degradation occurs during both storage and cycling because of several chemical and mechanical processes which ultimately lead to capacity fade through the loss of cyclable lithium and other active materials, and to power fade through the formation of interface films and the loss of electrical contact between certain materials (Barré et al. (2013)). This is summarized in Figure 3. The presence and extent of the different degradation mechanisms ultimately depend on the specific cell chemistry as well as storage and operating conditions; however, these mechanisms tend to interact with each other, which makes battery degradation prediction and modeling a difficult task (Vetter et al. (2005)). Nevertheless, there seem to be certain recurrent factors which accelerate aging in most lithium-ion batteries, such as overcharging, overdischarging, high and low

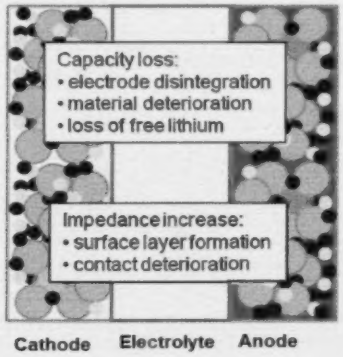

Figure 3: Summary of aging mechanisms
(Source : Hausbrand et al. (2015))

temperatures, high SOC during storage, large DOD, and high charging or discharging rates. These may be more easily incorporated into transportation planning problems without an expertise in electrochemistry. While some factors can be taken into account with simple model constraints (e.g., limiting the usable voltage or SOC window to avoid overcharging and overdischarging), the effect of others may require more elaborate degradation models (e.g., storage conditions, charging and discharging rates, temperature, DOD).

3.2 Useful battery lifetime degradation models

There exist different ways to estimate lithium-ion battery degradation depending on which performance attribute is being studied (capacity fade or resistance increase), which type of battery life is being considered (calendar or cycle life), and the overall modeling approach. Some of these approaches use electrochemical models, which rely heavily on theory to understand and predict the actual reactions causing degradation within the battery, while others use a more empirical approach to model battery aging, thus trying to establish relationships between battery aging and certain factors by using experimental data (Bashash et al. (2011)). Both electrochemical and empirical approaches have their drawbacks, notably that the former are very complex and too theoretical to be practically applied, while the latter require significant amounts of data and are only valid under specific experimental conditions (Xu (2013)). Semi-empirical models seek to combine the advantages of both previous approaches by combining theoretical principles with experimental results to attribute values to the fitting parameters of the models, thus being simpler than electrochemical models, while being applicable to broader conditions than empirical models (Xu (2013)).

Due to the very detailed and complex nature of electrochemical models, empirical and semi-empirical models seem like the most likely candidates in the context of transportation planning. The goal of this section is not to exhaustively survey such models, but rather to identify the most relevant ones for transportation planning problems. Also, since power capabilities of modern lithium-ion batteries are not problematic in BEVs, the following examples will focus on capacity fade models. Note that such empirical and semi-empirical methods measure the available capacity under reference conditions over the lifespan of the battery, thus eliminating the previously discussed variation of available capacity which can occur under different operating conditions.

Wang et al. (2011) have developed a semi-empirical degradation model for the cycle life of lithium iron phosphate cells, thus establishing a mathematical relationship linking capacity loss to the discharge C-rate, temperature and charge throughput. A discharge rate of one C is a measure of the discharging current associated with the delivered capacity when a fully charged battery reaches its cut-off voltage in one hour, and serves as the reference for expressing other discharging currents (Sauer (2009)). For example, if the one-hour discharge capacity of a battery is 10Ah, then $C = 10\text{A}$, $5C = 50\text{A}$, and $0.2C = 2\text{A}$. The charge throughput is the total amount of electrical charge processed through the cell. The model of Wang et al. (2011) provides a simple formula to account for different discharge rates via equation (1), in which Q_{loss} is the percentage of capacity loss, B is the pre-exponential factor, R is the gas constant, T is the absolute temperature, and A_h is the total charge throughput of the cell:

$$Q_{loss} = B \cdot \exp\left(\frac{-31700 + 370.3 \cdot C_{Rate}}{R \cdot T}\right) \cdot (A_h)^{0.55}. \tag{1}$$

Peterson et al. (2010) have developed an empirical degradation model for the cycle life of lithium iron phosphate cells as well, and have established a linear relationship between capacity fade and the discharged energy throughput (Wh) under a realistic PHEV driving duty cycle. Their results also show the difference in the degradation occurring in driving conditions (i.e., with a time-varying discharge current) and in static conditions (i.e., with a constant discharge current). This is important since empirical models are often validated under specific experimental operating conditions which may not adequately represent the dynamic load profiles to which electric vehicles are subject in reality. Models developed for static operating conditions therefore assume that the stress factors (e.g., charging and discharging rate, cycling DOD, average SOC and temperature) will be identical over the entire lifespan of the battery. Applying a degradation model that has not been developed

for dynamic operating conditions in a transportation planning problem thus requires making certain assumptions, such as the effect of time-varying stress factors during a certain horizon corresponds to the effect of their average values, and the effects of stress factors in different horizons are independent of each other.

Thus, ideally battery degradation models should be validated with data obtained under dynamic operating conditions, such as the semi-empirical ones proposed by Sarasketa-Zabala et al. (2014a) and Sarasketa-Zabala et al. (2014b) for calendar and cycling aging, respectively. These models establish mathematical relationships to link capacity loss to temperature and SOC for the calendar life model (equation (2)), as well as to DOD and charge throughput for the cycle life model (equations (3) and (4)). Both models were developed with experimental data of lithium iron phosphate cells, and validated under dynamic conditions. In the following calendar aging model, T is the storage temperature, t is the storage time in days, and α_1, β_1, α_2, and β_2 are fitting parameters:

$$Q_{loss} = \alpha_1 \cdot \exp\left(\beta_1 \cdot T^{-1}\right) \cdot \alpha_2 \cdot \exp\left(\beta_2 \cdot SOC\right) \cdot t^{0.5}. \tag{2}$$

The cycle aging model is expressed through the following capacity fade equations, in which DOD is the depth of discharge, Ah is the total charge processed through the battery, and α_3, β_3, α_4, β_4, γ_1, γ_2, and γ_3 are fitting parameters. Equation (3) is for a DOD ranging from 10% to 50%, while (4) is for all other DOD values. Parameter k is a correction factor for dynamic operating conditions and is thus equal to 1 if the cycling DOD is constant. The only problem arising in applying this cycle life model is that the swing of SOC during charging and discharging (DOD) is assumed to always occur around a middle SOC of 50%. However, the authors plan to combine the calendar and cycle life models into a unified degradation model which would be valid under varying operating conditions, and extend the cycle life model for other middle states of charge:

$$Q_{loss} = \left(\gamma_1 \cdot DOD^2 + \gamma_2 \cdot DOD + \gamma_3\right) \cdot k \cdot Ah^{0.87} \quad \text{for} \quad 10\% \leq DOD \leq 50\% \tag{3}$$

$$Q_{loss} = \left(\alpha_3 \cdot \exp(\beta_3 \cdot DOD) + \alpha_4 \cdot \exp(\beta_4 \cdot DOD)\right) \cdot k \cdot Ah^{0.65} \quad \text{for} \quad DOD < 10\% \quad \text{and} \quad DOD > 50\%. \tag{4}$$

Another interesting aspect of their work is the method for accounting for variations in operating conditions; they use the residual capacity resulting from previous conditions to determine the position on the capacity fade curve associated with the new conditions. This is illustrated

in Figure 4 for calendar life degradation with varying storage temperatures. For example, in Figure 4, the battery is initially stored at 10°C for approximately 600 days before the storage temperature changes to 40°C. Thus, the capacity fade curve for 10°C is first followed until the temperature switches to 40°C (arrow 1 in the figure). When this happens, a horizontal shift from the capacity fade curve for 10°C to the one for 40°C is performed in order to use the one for 40°C according to the accumulated capacity fade under the previous temperature. The capacity fade curve for 40°C is then followed during the total storage time at this temperature (arrow 2 in the figure). In the same vein, when the storage temperature then switches from 40°C to 20°C, the horizontal shift to the capacity fade curve for 20°C takes into account the accumulated degradation under all previous temperatures. Such an approach therefore requires making the assumption that the degradation resulting from new operating conditions is independent of the way the accumulated capacity fade was reached (Wenzl et al. (2013)).

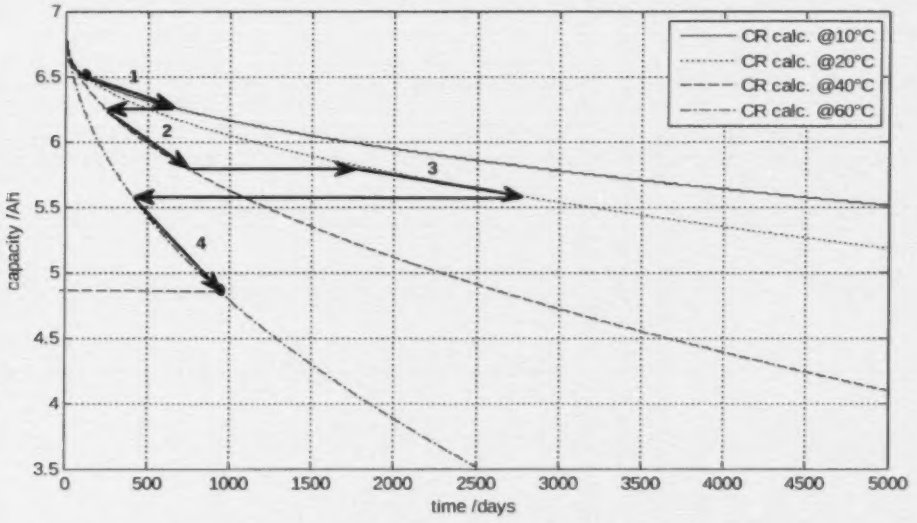

Figure 4: Using capacity fade curves under varying conditions
(Source : Wenzl et al. (2013))

Another approach for considering battery degradation (whether calendar or cycle aging) under varying conditions, is to consider the effect arising from operating conditions regarding a stress factor during a certain horizon relative to the total lifespan of the battery, if those same conditions were maintained throughout the battery's life. This approach was used by Hoke et al. (2011) to determine the loss of life ratios for the individual effects of temperature, average SOC, and cycling DOD on capacity fade, and for the effect of temperature on power fade. Using the assumption that the effects of these stress factors are independent, the

maximum between the total capacity fade costs and power fade costs is then chosen as the degradation cost associated with the planning horizon. Thus, the battery degradation cost c_{deg} over the considered horizon is obtained with equations (5) and (6), in which c_{bat} is the purchase cost of the battery, $c_{Q,T}$, $c_{Q,SOC}$, and $c_{Q,DOD}$ are capacity fade costs associated with temperature, SOC, and DOD respectively, and $c_{P,T}$ is the power fade cost associated with temperature. $\Delta L_{y,x}$ is the lifespan lost during the considered horizon due to fading characteristic y (i.e., capacity Q or power P) under the present conditions regarding stress factor x (i.e., T, SOC, or DOD), and $L_{y,x}$ is the total battery lifespan if the present conditions regarding stress factor x were maintained until fading characteristic y reached its end of life value. Readers may refer to the paper of Hoke et al. (2011) for more information on the determination of the different $c_{y,x}$ costs:

$$c_{deg} = \max c_{Q,T} + c_{Q,SOC} + c_{Q,DOD}, c_{P,T} \tag{5}$$

$$c_{y,x} = c_{bat} \cdot \frac{\Delta L_{y,x}}{L_{y,x}}. \tag{6}$$

Similar approaches (i.e., determining battery degradation costs via the product of relative loss of life and the battery's price) have also been used in a few transportation planning problems. Barco et al. (2013) applied a version of the model of Hoke et al. (2011) to their VRP with electric vehicles in the context of public transportation. Arslan et al. (2014) studied a minimum cost path problem for PHEVs in which they first determine the number of cycles which could be achieved for each DOD according to the battery's cycle life curve with respect to DOD, and then multiply the battery purchase cost by the inverse of the number of cycles for each possible DOD. Hence, they determine the parameters for the following quadratic degradation cost function in monetary units for any charging SOC swing δ_i at a node i along the path, in which a and b are parameters which depend on the specific cycle life versus DOD curve of the battery: $c_{deg} = a \cdot \delta_i^2 + b \cdot \delta_i$.

This kind of approach could also be extended to include more elaborate cycle life models as well. For example, Omar et al. (2014) developed an empirical relationship between the number of full cycles that could be achieved by lithium iron phosphate batteries and the charging rate used. Thus, a methodology similar to that of Arslan et al. (2014) could be employed in an electric vehicle routing problem with different charging options (e.g., Sassi et al. (2015); Felipe et al. (2014)) in order to determine a degradation cost per cycle associated with quickly charging the battery under a high charging rate. Moreover, Omar et al. (2014) also determined an empirical relationship between the number of cycles that

could be achieved by the battery with respect to DOD using a load profile representing dynamic operating conditions such as those encountered by electric vehicles. The resulting cycle life versus DOD curve could be combined with the approach of Han et al. (2014), who use the battery's acquisition cost and cycle life versus the DOD curve to develop a function representing wear costs per unit of energy going in or out of the battery according to the battery's SOC in order to account for different degradation rates occurring at different SOC levels.

Another interesting way of accounting for more specific cycling conditions than charge throughput is to use rainflow cycle counting to determine what should constitute cycles under irregular SOC driving profiles (Liu (2013)), as was done by Xu (2013) in his semi-empirical degradation model for capacity fade. The model extends that of Millner (2010) by accounting for irregular SOC profiles and isolating cycle and calendar aging. It considers stress factors such as DOD, SOC, C-rate, temperature and time. In order to determine the stress factors associated with each cycle in irregular SOC profiles, the rainflow cycle-counting method is applied to identify cycles and their respective amplitude (DOD), mean value (average SOC), begin time, and end time. Each cycle's C-rate and temperature are then determined, and their mean SOC and associated temperature are subsequently averaged to compute the horizon's overall SOC and temperature averages to be used in the calendar aging model alongside time. The fitting parameters of the model are determined with experimental data for lithium manganese oxide batteries.

Finally, accounting for overcharging degradation can essentially be achieved by modeling the recharging process as a CC-CV process (or CP-CV) rather than one linear charging function with time, since the CV phase eliminates the risk of reaching exceedingly high voltage levels which can damage the battery. However, this requires a method to monitor the non-linearly increasing SOC during the CV phase. In the context of transportation planning problems, Sweda et al. (2014) propose using an overcharging function that considers the extra amount of time required for charging the battery in the CV phase of a CC-CV charging scheme. The actual function is based on the experience of a Nissan Leaf driver and is used to determine optimal recharging policies along a certain path. Another method that has been employed in such problems is to use piecewise linear approximations for the charging curve according to experimental data. This technique was applied by Zündorf (2014) in his minimum cost path problem with different types of charging stations.

4. Instantaneous battery behaviour modeling

Modeling the battery as an equivalent electrical circuit is a tractable way to link the battery's terminal voltage, SOC and current. The simplest of these circuit models is illustrated in Figure 5; it consists of modeling the battery as an open-circuit voltage ($V_{OC}(SOC(t))$) source connected in series with an internal battery resistance $R(SOC(t))$.

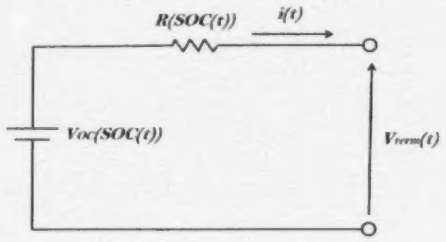

Figure 5: Simple battery equivalent circuit model, with current $i(t)$ direction reflecting discharging.

The open-circuit voltage of the battery corresponds to its voltage when there is no external load connected to it, i.e., when no current is flowing through the battery (Li and Ke (2011)). The battery's instantaneous actual voltage (or terminal voltage, $V_{term}(t)$) will be inferior and superior to its open-circuit voltage when it is being discharged and recharged, respectively, because of the current flowing out of it or into it (Larminie and Lowry (2003)). The open-circuit voltage and the internal resistance of the battery depend on factors such as SOC (Larminie and Lowry (2003)). The battery's terminal voltage at time t can thus be obtained with equation (7) from Larminie and Lowry (2003), in which $SOC(t)$ is the battery's SOC at time t, and $i(t)$ is the current flowing through the battery at time t, with the convention that the battery current is positive during discharging and negative during charging:

$$V_{term}(t) = V_{OC}(SOC(t)) - R(SOC(t)) \cdot i(t). \tag{7}$$

One way of establishing relationships between these circuit elements and such factors is to use empirical equations and find their fitting parameters with experimental data obtained by charging and discharging the battery. For example, Xu (2013) uses a circuit as in Figure 5 for lithium iron phosphate cells with empirical equations (8), (9), and (10); see Figure 6 for an example of these relations. The model also distinguishes between the resistance during discharging (R_d) and charging (R_c), and considers these as functions of SOC. The parameters in equations (8), (9) and (10) from Xu (2013) are determined experimentally by

Lam et al. (2011) and given in Appendix B:

$$V_{OC}(SOC) = a_1 e^{-a_2 SOC} + a_3 + a_4 SOC + a_5 e^{-\frac{a_6}{1-SOC}} \tag{8}$$

$$R_d(SOC) = b_{1d} SOC^4 + b_{2d} SOC^3 + b_{3d} SOC^2 + b_{4d} SOC + b_{5d} \tag{9}$$

$$R_c(SOC) = b_{1c} SOC^4 + b_{2c} SOC^3 + b_{3c} SOC^2 + b_{4c} SOC + b_{5c}. \tag{10}$$

With this model, assuming that the battery's SOC varies with time (i.e., $SOC(t)$), the

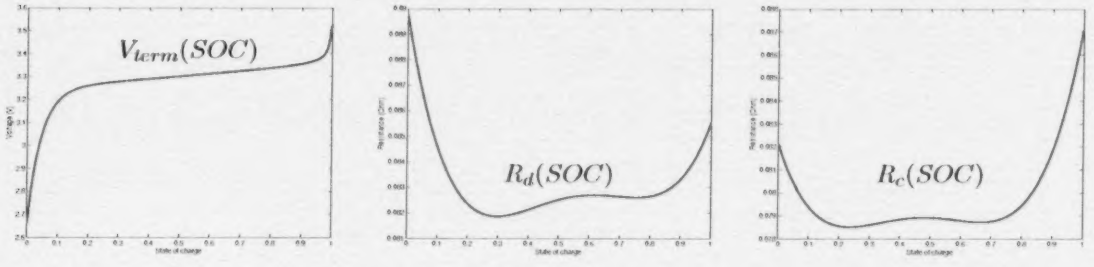

Figure 6: From left to right: plots of equations (8), (9) and (10), which describe voltage, discharging resistance and charging resistance, respectively, as functions of SOC.

instantaneous terminal voltage during discharging ($V_{term,d}(t)$) and charging ($V_{term,c}(t)$) is expressed through equations (11) and (12) respectively, which are adapted from Xu (2013):

$$V_{term,d}(t) = V_{OC}(SOC(t)) - R_d(SOC(t)) \cdot i(t) \tag{11}$$

$$V_{term,c}(t) = V_{OC}(SOC(t)) - R_c(SOC(t)) \cdot i(t). \tag{12}$$

Another approach is to use pre-established mathematical relationships to model fundamental relationships between terminal voltage, SOC and current (Li and Ke (2011)). The model of Tremblay et al. (2007), which is based on Shepherd's equation (Shepherd (1965)), is an example. It has the advantage of only requiring three points on the constant current discharge curve typically included in the battery's data sheets (as illustrated in Figure 7) to extract the model's parameters and it allows to develop a generic battery behaviour model for four battery types (including lithium-ion batteries). The approach of Tremblay et al. (2007) considers the following relationship between the open-circuit voltage and current:

$$V_{OC}(SOC(t)) = E_0 - \frac{K}{SOC(t)} + A \exp(-BQ(1 - SOC(t))). \tag{13}$$

In equation (13), E_0 is the battery constant voltage, K is the polarisation voltage, Q is the maximum battery capacity in ampere-hours, $i(t)$ is the instantaneous current, $SOC(t)$

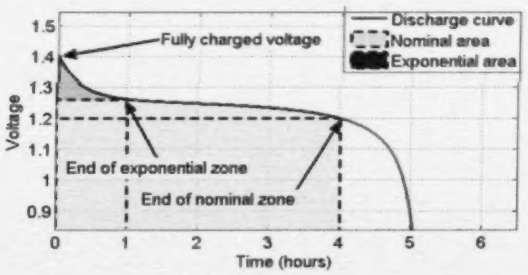

Figure 7: Typical constant current discharge curve
(Source : Tremblay et al. (2007))

is the present charge at time t with respect to maximum capacity Q, A is the exponential zone amplitude, and B is the exponential zone time constant inverse. Readers may refer to Tremblay et al. (2007) for the practical method to extract the parameters from the discharge curve. The model assumes that the internal resistance R in equation (7) is constant, that all parameters are identical during charging and discharging, that the temperature has no effect on the parameters, and that the minimum open-circuit voltage is zero.

Using this expression in (7) we obtain equation (14), which constitutes an alternative to (11) and (12) to describe the terminal voltage, for both charging and discharging:

$$V_{term}(t) = E_0 - \frac{K}{SOC(t)} + A\exp(-BQ(1 - SOC(t))) - R \cdot i(t). \tag{14}$$

There exist several additional ways of modeling the battery as an equivalent circuit, which vary according to trade-offs between accuracy and complexity (Chen and Rincón-Mora (2006)). For example, the model in Figure 5 assumes that the terminal voltage reacts instantaneously to an applied load, while in reality during sudden current variations there are both an instantaneous variation and a gradual one. These dynamic voltage responses under step current variations can be captured by adding parallel resistor-capacitor (RC) components to the circuit of Figure 5 (e.g., Chen and Rincón-Mora (2006), Liu (2013)).

In models based on mathematical relationships such as the one of Tremblay et al. (2007) previously discussed, such dynamic voltage responses during sudden current variations can be incorporated by using a filtered current flowing through a polarisation resistance, as proposed by Tremblay and Dessaint (2009). These authors further improved the model of Tremblay et al. (2007) by developing separate relationships for the four battery types during discharging and charging due to certain differences in voltage behaviours.

4.1 Discharging

In the context of routing electric vehicles for goods distribution, during discharging it is the required battery power that will determine the current to be supplied by the battery. In scenarios assuming a constant speed or infrequent and slow speed variations, the errors resulting from disregarding dynamic voltage responses are less significant (Larminie and Lowry (2003)). In such circumstances, a tractable circuit like that of Figure 5 seems like a practical way to account for fundamental battery discharging behaviour.

During discharging, the required mechanical power (P_M) can be found based on the road forces acting on the vehicle. The associated power output (or input in the case that regenerative braking is also considered) by the electric motor (P_E) and battery (P_B) can then be found according to their output (or input) efficiencies (Goeke and Schneider (2015)), as illustrated in Figure 8. Once the power profile required from the battery with respect to time is known (i.e., $P_B(t)$), it can be linked to its instantaneous terminal voltage $V_{term}(t)$ and current $i(t)$ with equation (15) from Larminie and Lowry (2003):

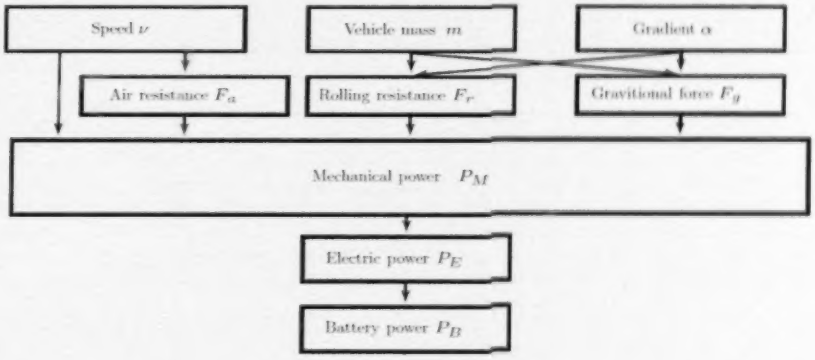

Figure 8: Schematic calculation of required battery power
(Source : Goeke and Schneider (2015))

$$P_B(t) = V_{term}(t) \cdot i(t). \tag{15}$$

Recalling that the terminal voltage can itself be modeled with equations (13) and (14), equation (15) can be reformulated as (16):

$$P_B(t) = (V_{OC}(SOC(t)) - R \cdot i(t)) \cdot i(t). \tag{16}$$

As in Moura et al. (2011), we define the rate of change of SOC with respect to time as

$$\dot{SOC}(t) = \frac{d}{dt}SOC(t) = -\frac{i(t)}{3600 \cdot Q}. \tag{17}$$

Note that since the maximum capacity Q is assumed to be in ampere-hours, it must be converted to coulombs by multiplying it by 3600, since current is expressed in coulombs per second. One can then solve the quadratic formula (18) resulting from equation (16) and thus find equation (19) for the instantaneous SOC rate of change, $\dot{SOC}(t)$, as in Moura (2011):

$$P_B(t) = V_{OC}(SOC(t)) \cdot i(t) - R \cdot i(t)^2 \tag{18}$$

$$\dot{SOC}(t) = -\frac{V_{OC}(SOC(t)) - \sqrt{V_{OC}(SOC(t)^2 - 4P_B(t)R}}{2 \cdot 3600QR}. \tag{19}$$

The expression of SOC with respect to time for the associated power profile can then be determined by solving the differential equation (19) with an initial SOC value, see Figure 9.

The same approach could also be used with a model considering the internal resistance R as a function of SOC (e.g., with equations (9) and (10)); it would yield comparable results to those shown in Figure 9. If using a degradation model considering charge throughput, the expression for the electrical current with respect to time (which can easily be found knowing the expression of $SOC(t)$) can be integrated over travel time to find the total charge throughput. If the degradation model also involves the discharging rate, one can then make the assumption that the C-rate corresponds to the one associated with the average current supplied (i.e., the charge throughput divided by the travel time). The expression for current with respect to time can also be discretized into segments during which the current does not vary significantly. The capacity fade curves associated with the average C-rate of each segment could then be used as in Figure 4 by replacing the horizontal axis with charge throughput and with variations in operating conditions being caused by changing C-rates rather than temperatures.

In addition, since the discharging process must be halted when the terminal voltage of the battery reaches a certain cut-off value V_{min}, it is possible to approximate the maximum available discharging power at any given moment t according to $SOC(t)$ with the relation linking terminal voltage, SOC and current. The maximum instantaneous discharging current $i_{max}(t)$ is the one which would result in the battery's terminal voltage $V_{term}(t)$ dropping to its known cut-off value V_{min}. With the model of Figure 5 and assuming that resistance R is constant, the following equations from Liu (2013) allow approximating the maximum

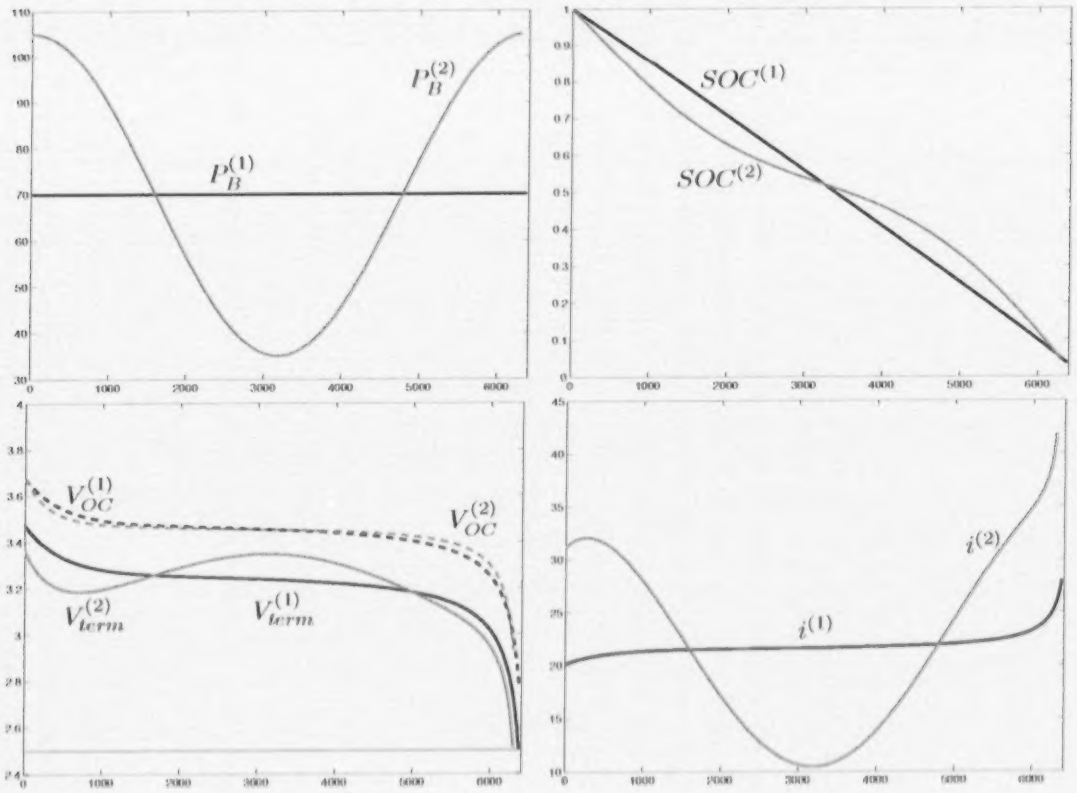

Figure 9: Numerical solutions of (19) for two different power profiles: a constant one, $P_B^{(1)}$, and an oscillating one, $P_B^{(2)}$ (top left diagram). In clockwise order starting from the top right diagram, for $j = 1, 2$, the corresponding states of charge $SOC^{(j)}$, currents $i^{(j)}$, open-circuit voltage $V_{OC}^{(j)}$ and terminal voltage $V_{term}^{(j)}$, as given by Equations (13) and (14) (right). The horizontal line in the voltage plot marks the cut-off voltage (V_{min} =2.5 V), the horizontal axis represents time (in seconds).

instantaneous available power $P_{B_{max}}(t)$:

$$\begin{aligned} V_{term}(t) &= V_{OC}(SOC(t)) - R \cdot i(t) \\ V_{min} &= V_{OC}(SOC(t)) - R \cdot i_{max}(t) \\ i_{max}(t) &= \frac{V_{OC}(SOC(t)) - V_{min}}{R}. \end{aligned}$$

Assuming that the maximum allowable discharging current $i_{max,limit}$ specified by the manufacturer is known, then if $i_{max}(t) \leq i_{max,limit}$, $P_{B_{max}}(t)$ is

$$P_{B_{max}}(t) = V_{term}(t) \cdot i_{max}(t)$$

$$= (V_{OC}(SOC(t)) - R \cdot i_{max}(t)) \cdot i_{max}(t)$$
$$= V_{min} \cdot i_{max}(t).$$

On the other hand, if $i_{max}(t) > i_{max,limit}$, then the maximum instantaneous available battery power (described in equation (20)) is the one that would require a current $i_{max,limit}$:

$$P_{B_{max}}(t) = (V_{OC}(SOC(t)) - R \cdot i_{max,limit}) \cdot i_{max,limit}. \tag{20}$$

Finally, it should be noted that the parameters of electrical circuit models are typically determined for single electrochemical cells, while battery packs are made of several parallel strings of cells connected in series. Assuming all cells in the pack are identical and that power P_{pack}, terminal voltage V_{pack}, and current i_{pack} at the pack level are evenly distributed among the cells (i.e., P_{cell}, V_{cell}, and i_{cell}), the relationships between these elements at the pack and cell level are given by equations (21), (22), and (23) from Xu (2013). N_p indicates the number of parallel strings and N_s indicates the number of cells connected in series per string:

$$P_{cell} = \frac{P_{pack}}{N_s \cdot N_p} \tag{21}$$

$$V_{cell} = \frac{V_{pack}}{N_s} \tag{22}$$

$$i_{cell} = \frac{i_{pack}}{N_p}. \tag{23}$$

Some cell models use parameters that can be directly extended to the pack level according to the cell's data sheets and the number of parallel strings in the pack and cells connected in series per string (e.g., MathWorks (2015)).

4.2 Charging

The battery models just described can be used to model the charging process since they allow monitoring the battery's terminal voltage and current throughout the process of CC-CV and CP-CV charging schemes (e.g., Marra et al. (2012)).

As discussed in Section 1.2, in a CC-CV charging process, the charging current is held constant during the first phase until the battery's voltage reaches a predefined maximum value V_{CV}; the SOC will therefore increase linearly with time, and the battery's terminal voltage can be monitored according to its relation with SOC and current. Once the terminal

voltage reaches its specified threshold, the charging process switches to the CV phase, during which the terminal voltage is held constant; the electrical current decreases exponentially with time until a minimal cut-off current value is reached, and the SOC's rate of change therefore continuously decreases. This is illustrated in Figure 10.

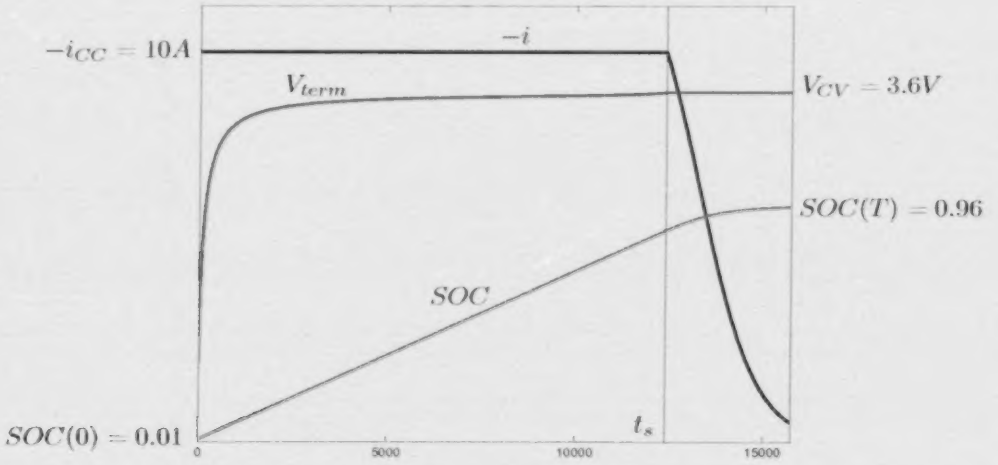

Figure 10: CC-CV charging scheme. The horizontal axis shows the time, the vertical axis is not in scale, in order to simultaneously illustrate the behaviour of current, voltage, and state of charge. The CC phase ($t < t_s$) is obtained explicitly from (24). The CV phase ($t > t_s$) is obtained as a numerical solution of the differential equation (26)–(28).

Thus, during the CC phase (i.e., until the terminal voltage reaches its specified threshold V_{CV}), the state of charge is given by

$$SOC(t) = SOC(0) - \frac{i_{CC} \cdot t}{3600 \cdot Q} \qquad \forall t \mid V_{term}(t) < V_{CV}, \tag{24}$$

where $SOC(0)$ is the known SOC at the moment the charging process begins, and i_{CC} is the known constant charging current (the battery current is assumed to be negative during charging).

The terminal voltage must be monitored during the CC phase in order to switch to CV charging when it reaches its known threshold V_{CV} and thus ensure the battery is not overcharged. This can be achieved by incorporating the expression for $SOC(t)$ from (24) and the constant charging current i_{CC} into equation (7), thus giving equation (25) in which $V_{OC}(SOC(t))$ can be determined with (13) if the resistance R is assumed to be constant:

$$V_{term}(t) = V_{OC}(SOC(t)) - R \cdot i_{CC} \qquad \forall t \mid V_{term}(t) < V_{CV}. \tag{25}$$

The same could be done by assuming that the internal resistance R varies with SOC as well, in which case equations (8) and (10) could be used for $V_{OC}(SOC(t))$ and $R(SOC(t))$.

Let t_s denote the time t for which $V_{term}(t) = V_{CV}$, which marks the switching time between CC and CV phase. The value of SOC upon entering this phase is simply $SOC(t_s) = SOC(0) - i_{CC} \cdot t_s / 3600 \cdot Q$. The relationship linking the terminal voltage to the battery's SOC and current (now a decreasing function of time, $i(t)$) allows one to establish a differential equation which can be solved to find SOC as a function of time during the CV phase, according to the initial value $SOC(t_s)$ and the maintained voltage value V_{CV}. Recalling the relationship between the rate of change of SOC and electrical current (17) results in the following equations for the CV phase:

$$i(t_s) = i_{CC} \tag{26}$$

$$\begin{aligned} V_{CV} &= V_{OC}(SOC(t)) - R \cdot i(t) \quad \forall t \geq t_s \\ &= V_{OC}(SOC(t)) + R \cdot 3600 \cdot Q \cdot \dot{SOC}(t) \end{aligned} \tag{27}$$

$$\dot{SOC}(t) = \frac{V_{CV} - V_{OC}(SOC(t))}{R \cdot 3600 \cdot Q}. \tag{28}$$

Once the expression for $SOC(t)$ has been determined, the one for $i(t)$ can be easily deduced during the CV phase and the charging process can be terminated once it falls below a certain current threshold i_{min}. One can intuitively understand why the SOC increases concavely during the CV phase by recalling that the battery's open-circuit voltage increases with SOC and that a larger current implies a larger difference between the battery's open-circuit and terminal voltage (with the latter superior to the former during charging). The battery's terminal voltage is held constant during CV, so that following an infinitesimal time increment after entering the CV phase, the SOC will increase by the amount corresponding to the current used in the CC phase. Since the SOC will have increased, so will the open-circuit voltage, but since the terminal voltage must remain constant, the current will have to decrease (Bergveld (2001)). Hence following another infinitesimal time increment, the SOC will have further increased, but at a slower pace due to the current decrease, thus requiring the current to further diminish, and so on until the current reaches its termination value.

The other advantage of considering the charging process in such a way is that it allows for monitoring the power being retrieved from the grid more accurately, and hence for the development of more realistic grid capacity constraints in routing problems which allow central depot recharging. For example, the power on the grid side can be monitored by linking the instantaneous grid charging power $P_{grid}(t)$ to the required battery power $P_B(t)$

according to the charging efficiency η (Marra et al. (2012)). Since the current is held constant while the terminal voltage increases during the CC phase, and since $P_B(t) = V_{term}(t) \cdot i_{cc}$ during this phase, both P_B and P_{grid} will increase (in absolute values) with time until reaching the CV phase. This is illustrated in Figure 11 for a CC-CV scheme with an initial charging power level of 3.7 kW and an initial SOC of 60%.

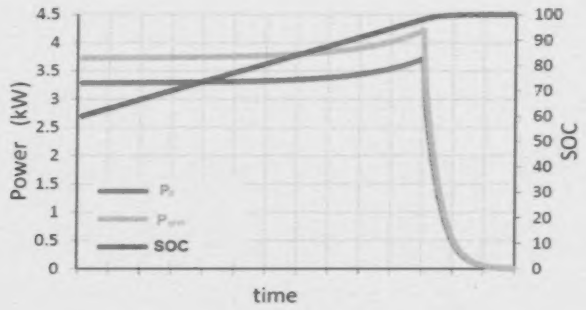

Figure 11: Charging power during CC-CV charging scheme
(Source : Marra et al. (2012))

This also enables us to determine the charging current i_{CC} that will be applied to the battery during the CC phase if the charger offers an adjustable initial power level $P_{grid}(0)$. Denoting $V_0 := V_{OC}(SOC(0))$, the following equations describe the relation between $P_{grid}(t)$ and $P_B(t)$, as well as how to find i_{CC}, assuming the initial SOC and charging power to be known (i.e., $SOC(0)$ and $P_{grid}(0)$):

$$\begin{aligned} P_B(t) &= \eta \cdot P_{grid}(t) \\ P_B(0) &= \eta \cdot P_{grid}(0) = V_{term}(0) \cdot i_{CC} = (V_0 - R \cdot i_{CC}) \cdot i_{CC} \\ i_{CC} &= \frac{V_0 - \sqrt{V_0^2 - 4P_B(0)R}}{2R}. \end{aligned} \tag{29}$$

On the other hand, in the absence of an increase in the grid's power output throughout the charging process, the battery can be charged under a CP-CV charging process (Marra et al. (2012)). According to the constant power output from the grid and the charging efficiency, the power applied to the battery during the CP phase can be found with equation (29), and the functions for SOC and current (which decreases with time since the terminal voltage increases but the power must remain constant) can be found with equation (19) for a constant power P_B instead of $P_B(t)$, assumed to be negative during charging. Once the terminal voltage reaches its threshold, the same method as for the CV phase in the CC-CV

scheme can be applied to express SOC as a function of time.

4.3 Simplifications

Evidently, there exist several different ways of modeling the behaviour of a battery during discharging and charging, ultimately varying according to trade-offs between accuracy and complexity. Nevertheless, some simplifications can also be made. A few of these are now discussed.

4.3.1 Time discretization

In order to avoid having to deal with continuous temporal functions for SOC and current that must be determined by solving differential equations, time can always be discretized into short intervals during which it is assumed that the battery's power, terminal voltage and current remain constant. This eliminates the need both for solving differential equations and for integrating current to find charge throughputs. Knowing the initial SOC at the start of the horizon and the length Δt of each time step, the SOC at the beginning of each time step k could thus be determined according to the current of the previous one, as expressed in equation (30) from Dekkiche (2008):

$$SOC_{k+1} = SOC_k - \frac{\Delta t}{3600 \cdot Q} \cdot i_k. \tag{30}$$

Similarly, the charge throughput of a period will correspond to the product of its current and duration. With a tractable circuit model in which the battery is considered as a SOC-dependent open-circuit voltage connected in series with a constant internal resistance, the terminal voltage of each time step will correspond to

$$V_{term_k} = V_{OC}(SOC_k) - R \cdot i_k.$$

As a result, for a given SOC_k and discharging or charging battery power P_k, the current of each time step will be

$$i_k = \frac{V_{OC}(SOC_k) - \sqrt{V_{OC}(SOC_k)^2 - 4P_kR}}{2R}. \tag{31}$$

During the CV phase of charging, the current of each period is then determined according

to the constant terminal voltage V_{CV} and the SOC at the start of the period:

$$V_{CV} = V_{OC}(SOC_k) - R \cdot i_k$$
$$i_k = \frac{V_{OC}(SOC_k) - V_{CV}}{R}.$$

Note that such time discretization can also be used to solve the previous differential equations numerically with the explicit Euler method.

4.3.2 Constant open-circuit voltage

Although it seems relevant to closely monitor the battery's terminal voltage, current, and SOC during charging in the context of goods distribution with electric vehicles in order to determine realistic charging times, this seems somewhat less reasonable in a transportation planning problem to simulate the battery's voltage, current and SOC in real time. Doing so while simultaneously optimizing delivery routes and respecting their associated operational constraints may lead to a problem that is simply too large for practical purposes. However, since some lithium-ion batteries such as those with a lithium iron phosphate cathode have a relatively flat open-circuit voltage curve for a large SOC range, while the battery is discharging one could assume that it has a fixed open-circuit voltage, e.g., its average value with respect to SOC. A circuit model with a constant internal resistance can then be used to further simplify the analysis. With such a model, if in addition the discharging power is assumed to be constant, the discharging current will also be constant for the required power output. As a result, SOC can be assumed to decrease linearly, and the value of degradation model variables such as charge throughput and C-rate can be easily determined.

4.3.3 Peukert equation

If the load can be regarded as a constant discharge current, the Peukert equation offers a practical method to account for variations in available capacity according to the discharging current. The following discussion is based on principles and equations from Larminie and Lowry (2003) and Khajepour et al. (2014). A battery's Peukert capacity C_p is assumed to be the available capacity in ampere-hours of a battery under a constant discharge current of 1A. The battery's constant Peukert coefficient k is used to establish a relationship between its Peukert capacity and any constant discharge current i and associated discharge time t_{cut} (i.e., the elapsed time in hours from a fully charged state before the terminal voltage reaches its cut-off value when discharged with constant current i):

$$C_p = i^k \cdot t_{cut}.$$

The coefficient k can be found with two known capacity ratings (C_1 and C_2) for the battery and their associated discharge time in hours (t_{cut_1} and t_{cut_2}). First, the discharge current (i_1 and i_2) for each capacity rating can be computed:

$$i_1 = \frac{C_1}{t_{cut_1}}, \qquad i_2 = \frac{C_2}{t_{cut_2}}.$$

We can then use this information to find the Peukert coefficient k since the right-hand side of both following equations must be equivalent:

$$C_p = i_1^k \cdot t_{cut_1}, \qquad C_p = i_2^k \cdot t_{cut_2}.$$

The coefficient k is thus

$$k = \frac{\log t_{cut_2} - \log t_{cut_1}}{\log i_1 - \log i_2}.$$

The available capacity $C_a(i)$ in ampere-hours and discharge time $t_{cut}(i)$ in hours for any constant discharge current i can then be estimated through the following equations:

$$t_{cut}(i) = \frac{C_p}{i^k}$$

$$C_a(i) = t_{cut}(i) \cdot i = \frac{C_p}{i^{k-1}}.$$

It is also possible to assume that with a time-varying discharge current $i(t)$, the level of discharge of the battery can be estimated with respect to the constant Peukert capacity C_p according to the integral of $i^k(t)$ over time. Assuming a positive current during discharge, if the instantaneous level of discharge $D(t)$ is defined as a value ranging from 0 (i.e., fully charged state) to 1 (i.e., when the cut-off voltage has been reached), and if the initial level of discharge D_0 is known, then $D(t)$ can be defined as

$$D(t) = D_0 + \frac{\int_0^t i^k(t)}{3600 \cdot C_p}.$$

The Peukert capacity is multiplied by 3600 to convert it to the same unit as $i^k(t)$

(coulombs). The instantaneous variation of the level of discharge is thus

$$\frac{dD(t)}{dt} = \frac{i^k(t)}{3600 \cdot C_p}.$$

This is a simple but interesting capacity modeling approach since it provides a method to estimate variations of available capacity without having to monitor the terminal voltage of the battery. The coefficient k for lithium-ion batteries typically varies between 1 and 1.09, where a value of 1 indicates that there is no loss of capacity under higher discharge currents (Omar et al. (2012)). Estimations of available capacity based on the Peukert relationship can also be further extended to incorporate the effect of other factors (e.g., temperature and cycle life) on the Peukert coefficient (Omar et al. (2013)).

5. Conclusions

The goal of this article was not to advance the science of battery monitoring and degradation, but rather to model these features so as to provide applicable knowledge to the growing community of researchers involved in the planning of goods distribution by electric vehicles. Several lithium-ion battery degradation mechanisms and specific storage and operating conditions that affect their lifespan were described, as well as a few useful degradation models. In addition, some existing battery models and principles were investigated and aggregated in order to account for fundamental battery behaviour during discharging and charging. We have shown that battery degradation and behaviour are quite complex phenomena to model, and that several different modeling approaches are available. We have concluded that empirical approaches allow for the development of capacity fade equations which are more easily employed without an expertise in electrochemistry. In the same vein, modeling the battery as an equivalent circuit appears to be a tractable way to describe basic battery characteristics during charging and discharging.

Moreover, our simultaneous investigation of both battery degradation and behaviour leads to a few intuitive insights which should be of interest from a fleet management perspective in the context of goods distribution with electric vehicles. For example, since calendar aging occurs faster when the battery is stored at a higher SOC, in terms of battery health, the charging of fleet vehicles should always be performed as closely as possible to their departure time. Another insight concerns the charging time and the required SOC upon departure. If different charging rate options are available at the depot for the CC phase during CC-CV charging, the use of a higher charging rate will cause the SOC to increase more quickly

during the CC phase, but the terminal voltage will reach its maximum value at a lower SOC (Lam (2011)). Since the purpose of using a higher charging current is to quickly charge the battery, in such cases it seems logical to terminate charging after the CC phase. Hence, if the CV phase is not performed, there exists a trade-off between the elapsed time and the SOC at the end of the CC phase according to the charging rate used.

Finally, we believe that some of our findings can be used in the context of goods distribution with electric vehicles to develop charging and discharging policies which ensure that battery health is preserved both in the short and long term, the latter being treated from a more strategic perspective. For instance, operating the battery outside its specified voltage range will quickly cause severe overcharging and overdischarging degradation, and should therefore always be avoided (Lam (2011)). However, storing the battery overnight at a higher rather than a lower SOC has a much smaller effect, and hence does not need to be as tightly constrained. The same could be said about cycling the battery with a large DOD or with large charging and discharging rates. The incorporation of such stress factors in transportation planning problems is not so straightforward, but the use of calendar and cycle aging models should allow for the development of certain habits that can prolong battery life.

Acknowledgments

This research was partly supported by the Canadian Natural Sciences and Engineering Research Council under grants 463834-2014, 436014-2013 and 2015-06189. This support is gratefully acknowledged. Thanks are also due to Olivier Tremblay for sharing his knowledge of battery modeling with us.

Appendix A. Glossary

Anode: The electrode of a cell at which the oxidation reaction (i.e., loss of electrons) occurs during discharging.

Available capacity (C_a): The amount of charge that can be discharged from a fully charged battery before the terminal voltage reaches its cut-off value. The available capacity is reduced when the battery is discharged with larger currents. Capacity is expressed in ampere-hours (Ah), with one Ah equivalent to a current of one A supplied during one hour

(i.e., A = C/s = $\frac{1}{3600}$ Ah/s). If the terminal voltage reaches its cut-off value at time t_{cut} when discharged from a fully charged state at time t_0, the available capacity in Ah is

$$C_a = \int_{t_0}^{t_{cut}} \frac{i(t)}{3600} \cdot dt.$$

Available energy (E_a): The amount of energy that can be supplied from a fully charged battery before the terminal voltage reaches its cut-off value, expressed in watt-hours (Wh). If the terminal voltage reaches its cut-off value at time t_{cut} when discharged from a fully charged state at time t_0, the available energy is

$$E_a = \int_{t_0}^{t_{cut}} P_B(t) \cdot dt = \int_{t_0}^{t_{cut}} V_{term}(t) \cdot i(t) \cdot dt.$$

Battery current ($i(t)$): The electrical current flowing through the battery at time t, assumed to be positive during discharging and negative during charging in this article. The battery current is expressed in amperes (A), with one A equivalent to one coulomb (C) per second.

Battery electric vehicle (BEV) : A vehicle that is propelled by an electric motor and only uses the power provided by its battery that can be charged from the electricity grid.

Battery power ($P_B(t)$): The instantaneous power supplied by or to the battery, equivalent to the product of the battery's instantaneous terminal voltage and current, and expressed in watts (W):

$$P_B(t) = V_{term}(t) \cdot i(t).$$

Cathode: The electrode of a cell at which the reduction reaction (i.e., gain of electrons) occurs during discharging.

C-rate: A discharge rate of one C is a measure of the discharging current associated with the available capacity when a fully charged battery reaches its cut-off voltage in one hour, and serves as the reference for expressing other discharging currents. If the one-hour discharge capacity of a battery is 10 Ah, then $C = 10\text{A}$, $5C = 50\text{A}$, and $0.2C = 2\text{A}$.

Cut-off voltage (V_{min}): The minimum allowable terminal voltage value. Discharging must be halted when the terminal voltage, which decreases while the battery is discharged, reaches this value.

Electrolyte: The medium that allows ions to be displaced between the anode and the cathode within a cell while electrons flow through an external electrical circuit.

Depth of discharge (DOD): The proportion of electrical charge discharged or charged during a cycle with respect to the maximum possible charge the battery can hold.

Hybrid electric vehicle (HEV): A vehicle that uses an internal combustion engine and an electric motor for propulsion, as well as a battery for electrical energy storage.

Lithium-ion battery: Several lithium-ion cells connected in series and parallel to reach the desired voltage and capacity.

Lithium-ion cell: An electrochemical device in which lithium ions are displaced back and forth between two electrodes in order to transform the stored chemical energy into electrical energy during discharging, and the provided electrical energy into chemical energy during charging.

Maximum charge voltage (V_{CV}): The maximum allowable terminal voltage value during charging, expressed in volts (V) and indicating when the charging scheme switches from the constant current phase to the constant voltage phase.

Memory effect: The gradual loss of available capacity when certain types of batteries are frequently recharged without being fully discharged.

Open-circuit voltage ($V_{OC}(SOC(t))$): The voltage between the battery terminals when there is no load connected (i.e., when no current is flowing through the battery), expressed in volts (V). The open-circuit voltage depends on the SOC of the battery at time t.

Plug-in hybrid electric vehicle (PHEV): A hybrid electric vehicle with a battery that can be charged from the electricity grid.

Specific energy: The approximate amount of energy stored per unit of battery mass, expressed in watt-hours per kilogram (Wh/kg).

Specific power: The approximate amount of available power per unit of battery mass,

expressed in watts per kilogram (W/kg).

State of charge ($SOC(t)$): The proportion of electrical charge inside the battery at time t with respect to the maximum possible charge Q it can hold.

Terminal voltage ($V_{term}(t)$): The voltage between the battery terminals at time t when a load is connected (i.e., when a current is flowing through the battery), expressed in volts (V). The terminal voltage is superior and inferior to the open-circuit voltage while charging and discharging, respectively.

Appendix B. Parameter values

In this section, we list the numerical values used to produce Figures 6, 9, and 10.

Figure 6 uses parameter values from Lam et al. (2011); (left) is the plot of equation (8) with parameters

$$a_1 = -0.5863, \quad a_2 = 21.90, \quad a_3 = 3.414, \quad a_4 = 0.1102, \quad a_5 = -0.1718, \quad a_6 = 0.008;$$

(center) is the plot of equation (9) with parameters

$$b_{1d} = 0.1298, \quad b_{2d} = -0.2892, \quad b_{3d} = 0.2273, \quad b_{4d} = -0.07216, \quad b_{5d} = 0.0898;$$

(right) is the plot of equation (10) with parameters

$$b_{1c} = 0.1369, \quad b_{2c} = -0.2518, \quad b_{3c} = 0.1609, \quad b_{4c} = -0.041, \quad b_{5c} = 0.0821.$$

Figure 9 (top left): Final time: $T = 6370$ seconds, $P_B^{(1)}(t) \equiv 70$, $P_B^{(2)}(t) = 70(1 + 0.5\cos(2\pi t/T))$; (top right): numerical solution of Equation (19) with $R = 0.01$, $Q = 40$, and $V_{OC}(SOC)$ given by (13) with $E_0 = 3.5$, $K = 0.025$, $A = 0.2$, $B = 0.375$ (parameter values from Marra et al. (2012)); (bottom left) is the plot of (13) and (14); (bottom right) the current is obtained from (18), as in (31).

Figure 10: (CC-phase): $i_{cc} = -10A$, $SOC(t)$ is obtained from (24), $V_{term}(t)$ from (25), with V_{OC} given by (13) with $R = 0.01$. (CV-phase): SOC is obtained from (28) with $Q = 40$ and $V_{CV} = 3.6V$.

The numerical solutions of the ordinary differential equations (19) and (28) are obtained

with the `ode45` solver in MATLAB.

References

A123 systems. 2015. Energy storage for commercial and off-highway vehicles. URL `http://www.a123systems.com/solutions-transportation-commercial-vehicles.htm`. Last accessed 28/6/2015.

ACEA (European Automobile Manufacturers' Association). 2013. Differences Between Diesel and Petrol. URL `http://www.acea.be/news/article/differences-between-diesel-and-petrol`. Last accessed 28/5/2015.

Afroditi, A., M. Boile, S. Theofanis, E. Sdoukopoulos, D. Margaritis. 2014. Electric vehicle routing problem with industry constraints: trends and insights for future research. *Transportation Research Procedia* **3** 452–459.

Agubra, V., J. Fergus. 2013. Lithium ion battery anode aging mechanisms. *Materials* **6**(4) 1310–1325.

Amine, K., J. Liu, I. Belharouak. 2005. High-temperature storage and cycling of C-LiFePO4/graphite Li-ion cells. *Electrochemistry Communications* **7**(7) 669–673.

Aravindan, V., J. Gnanaraj, S. Madhavi, H.-K. Liu. 2011. Lithium-ion conducting electrolyte salts for lithium batteries. *Chemistry European Journal* **17** 14326–14346.

Arora, P., R.E. White, M. Doyle. 1998. Capacity fade mechanisms and side reactions in lithium-ion batteries. *Journal of the Electrochemical Society* **145**(10) 3647–3667.

Arslan, O., B. Yıldız, O.E. Karaşan. 2014. Minimum cost path problem for plug-in hybrid electric vehicles. *Transportation Research Part E* **80** 123–141.

AustriaTech. 2014. Electric fleets in urban logistics: Improving urban freight efficiency in small and medium-sized historic towns. Published as part of the ENCLOSE project, funded by Intelligent Energy Europe (IEE), Vienna, Austria. URL `http://www.austriatech.at/files/get/834747f18fdcc9538376c9314a4d7652/austriatech_electricfleets_broschuere.pdf`. Last accessed 10/6/2015.

Balqon Corporation. 2013. M100 product specifications. URL `http://www.balqon.com/wp-content/uploads/2013/09/m100_brochure_2013.pdf`. Last accessed 19/6/2015.

Balqon Corporation. 2015. Mule M100 electric truck. URL `http://www.balqon.com/electric-vehicles/mule-m100/`. Last accessed 15/6/2015.

Barco, J., A. Guerra, L. Muñoz, N. Quijano. 2013. Optimal routing and scheduling of charge for electric vehicles: Case study. Working paper. Universidad de los Andes, Bogotá, Colombia. URL `http://arxiv.org/ftp/arxiv/papers/1310/1310.0145.pdf`. Last accessed 12/6/2015.

Barré, A., B. Deguilhem, S. Grolleau, M. Gérard, F. Suard, D. Riu. 2013. A review on lithium-ion battery ageing mechanisms and estimations for automotive applications. *Journal of Power Sources* **241** 680–689.

Bashash, S., S.J. Moura, J.C. Forman, H.K. Fathy. 2011. Plug-in hybrid electric vehicle charge pattern optimization for energy cost and battery longevity. *Journal of Power Sources* **196** 541–549.

Bergveld, H.J. 2001. Battery management systems: Design by modelling. Ph.D thesis, University of Twente, Enschede, The Netherlands.

Bektaş, T., G. Laporte. 2011. The pollution-routing problem. *Transportation Research Part B* **45**(8) 1232–1250.

Belt, J.R., C.D. Ho, C.G. Motloch, T.J. Miller, T.Q. Duong. 2003. A capacity and power fade study of Li-ion cells during life cycle testing. *Journal of Power Sources* **123**(2) 241–246.

Boulder Electric Vehicle. 2015. 1000-series master brochure. URL `http://www.boulderev.com/docs/1000%20Master%20Brochure.pdf`. Last accessed 13/6/2015.

Bruce, P.G., S.A. Freunberger, L.J. Hardwick, J-M. Tarascon. 2012. Li-O2 and Li-S batteries with high energy storage. *Nature Materials* **11**(1) 19–29.

Bruglieri, M., F. Pezzella, O. Pisacane, S. Suraci. 2015. A variable neighborhood search branching for the electric vehicle routing problem with time windows. *Electronic Notes in Discrete Mathematics* **47** 221–228.

Campbell, R. 2011. Battery Characterization and Optimization for use in Plug-in Hybrid Electric Vehicles: Hardware-in-the-loop duty cycle testing. Master's thesis, Queen's University, Kingston, Canada.

Chen, M., G.A. Rincón-Mora. 2006. Accurate electrical battery model capable of predicting runtime and IV performance. *IEEE Transactions on Energy Conversion* **21**(2) 504–511.

Cluzel, C., C. Douglas. 2012. Cost and performance of EV batteries. Element Energy, Axeon and EaStCHEM, commissioned by The Committee on Climate Change. URL `http://www.element-energy.co.uk/wordpress/wp-content/uploads/2012/06/CCC-battery-cost_-Element-Energy-report_March2012_Finalbis.pdf`. Last accessed 29/5/2015.

Conrad, R.G., M.A. Figliozzi. 2011. The recharging vehicle routing problem. In: Doolen, T., Van Aken, E., eds. *Proceedings of the 2011 Industrial Engineering Research Conference*. Reno, Nevada.

Davis, B.A., M.A. Figliozzi. 2013. A methodology to evaluate the competitiveness of electric delivery trucks. *Transportation Research Part E* **49**(1) 8–23.

Dekkiche, A. 2008. Modèle de batterie générique et estimation de l'état de charge. Master's thesis, École de technologie supérieure, Montreal, Canada.

Demir, E., T. Bektaş, G. Laporte. 2011. A comparative analysis of several vehicle emission models for road freight transportation. *Transportation Research Part D* **16**(5) 347–357.

Demir, E., T. Bektaş, G. Laporte. 2014. A review of recent research on green road freight transportation. *European Journal of Operational Research* **237**(3) 775–793.

den Boer, E., S. Aarnink, F. Kleiner, J. Pagenkopf. 2013. Zero emission trucks: An overview of state-of-the-art technologies and their potential. CE Delft and DLR, commissioned by the International Council on Clean Transportation (ICCT). URL `http://www.cedelft.eu/?go=home.downloadPub&id=1399&file=CE_Delft_4841_Zero_emissions_trucks_Def.pdf`. Last accessed 12/6/2015.

Dinger, A., R. Martin, X. Mosquet, M. Rabl, D. Rizoulis, M. Russo, G. Sticher. 2010. Batteries for electric cars: Challenges, opportunities, and the outlook to 2020. The Boston Consulting Group. URL `https://www.bcg.com/documents/file36615.pdf`. Last accessed 10/6/2015.

Duleep, G., H. van Essen, B. Kampman, M M. Grünig. 2011. Impacts of electric vehicles - deliverable 2: Assessment of electric vehicle and battery technology. CE Delft, ICF International, and Ecologic, commissioned by the European Commission. URL `http://www.cedelft.eu/?go=home.downloadPub&id=1153&file=4058_D2defreportHvE_1314726004.pdf`. Last accessed 8/6/2015.

Electric Vehicles International. 2015. EVI Medium Duty Truck Specification Sheet. URL `http://www.evi-usa.com/LinkClick.aspx?fileticket=SyZhwUVqNJs%3d&tabid=83`. Last accessed 16/5/2015.

Electrification Coalition. 2013. State of the plug-in electric vehicle market. URL `http://www.electrificationcoalition.org/sites/default/files/EC_State_of_PEV_Market_Final_1.pdf`. Last accessed 5/6/2015.

Felipe, Á., M.T. Ortuño, G. Righini, G. Tirado. 2014. A heuristic approach for the green vehicle routing problem with multiple technologies and partial recharges. *Transportation Research Part E* **71** 111–128.

Feng, W., M. Figliozzi. 2013. An economic and technological analysis of the key factors affecting the competitiveness of electric commercial vehicles: A case study from the USA market. *Transportation Research Part C* **26** 135–145.

Gallo, J-B., J. Tomić. 2013. Battery electric parcel delivery truck testing and demonstration. California Hybrid, Efficient and Advanced Truck Research Center (CalHEAT). URL `http://www.calstart.org/Libraries/CalHEAT_2013_Documents_Presentations/Battery_Electric_Parcel_Delivery_Truck_Testing_and_Demonstration.sflb.ashx`. Last accessed 12/6/2015.

Gerssen-Gondelach, S.J., A.P.C. Faaij. 2012. Performance of batteries for electric vehicles on short and longer term. *Journal of Power Sources* **212** 111–129

Goeke, D., M. Schneider. 2015. Routing a mixed fleet of electric and conventional vehicles. *European Journal of Operational Research* **245**(1) 81–99.

Gonzalez-Feliu, J., F. Semet, J-L. Routhier, eds. 2014. *Sustainable Urban Logistics: Concepts, Methods and Information Systems*. Springer, Berlin Heidelberg.

Han, S., S. Han, H. Aki. 2014. A practical battery wear model for electric vehicle charging applications. *Applied Energy* **113** 1100–1108.

Hausbrand, R., G. Cherkashinin, H. Ehrenberg, M. Gröting, K. Albe, C. Hess, W. Jaegermann. 2015. Fundamental degradation mechanisms of layered oxide Li-ion battery cathode materials: Methodology, insights and novel approaches. *Materials Science and Engineering B* **192** 3–25.

Hiermann, G., J. Puchinger, R.F. Hartl. 2014. The electric fleet size and mix vehicle routing problem with time windows and recharging stations. Working Paper. URL `http://prolog.univie.ac.at/research/publications/downloads/Hie_2015_638.pdf`. Last accessed 29/5/2015.

Hoke, A., A. Brissette, D. Maksimović, A. Pratt, I. Labs, K. Smith. 2011. Electric vehicle charge optimization including effects of lithium-ion battery degradation. *2011 IEEE Vehicle Power and Propulsion Conference (VPPC)*. IEEE, Chicago, Illinois, 1–8.

International Energy Agency (IEA), Electric Vehicles Initiative (EVI). 2013. Global EV outlook - Understanding the electric vehicle landscape to 2020. URL `http://www.iea.org/publications/globalevoutlook_2013.pdf`. Last accessed 12/6/2015.

Kamarianakis, Y., H.O. Gao, B.A. Holmén, D.B. Sonntag. 2011. Robust modeling and forecasting of diesel particle number emissions rates. *Transportation Research Part D* **16**(6) 435–443.

Khajepour, A., S. Fallah, A. Goodarzi. 2014. *Electric and Hybrid Vehicles - Technologies, Modeling, and Control: A Mechatronic Approach*. Wiley, Chichester, United Kingdom.

Koç, C., T. Bektaş, O. Jabali, G. Laporte. 2014. The fleet size and mix pollution-routing problem. *Transportation Research Part B* **70** 239–254.

Kopfer, H.W., H. Kopfer. 2013. Emissions minimization vehicle routing in dependence of different vehicle classes. In: Kreowski, H-J., Scholz-Reiter, B., Thoben, K-D., eds. *Dynamics in Logistics – Proceedings of LDIC 2012*. Lecture Notes in Logistics, Springer, Berlin Heidelberg, 49–58.

Kopfer, H.W., J. Schönberger, H. Kopfer. 2014. Reducing greenhouse gas emissions of a heterogeneous vehicle fleet. *Flexible Services and Manufacturing Journal* **26** 221–248.

Lam, L. 2011. A practical circuit-based model for state of health estimation of li-on battery cells in electric vehicles. Master's thesis, Delft University of Technology, Delft, The Netherlands.

Lam, L., P. Bauer, E. Kelder. 2011. A practical circuit-based model for Li-ion battery cells in electric vehicle applications. *2011 IEEE 33rd International Telecommunications Energy Conference (INTELEC)*. IEEE, Amsterdam, The Netherlands, 1–9.

Larminie, J., J. Lowry. 2003. *Electric Vehicle Technology Explained*. Wiley, Chichester.

Lebeau, P., C. De Cauwer, J. Van Mierlo, C. Macharis, W. Verbeke, T. Coosemans. 2015. Conventional, hybrid, or electric vehicles: Which technology for an urban distribution centre? *The Scientific World Journal*, Article ID 302867.

Lee, D.Y., V.M. Thomas, M.A. Brown. 2013. Electric urban delivery trucks: Energy use, greenhouse gas emissions, and cost-effectiveness. *Environmental Science & Technology* **47**(14) 8022–8030.

Li, S., B. Ke. 2011. Study of battery modeling using mathematical and circuit oriented approaches. *2011 IEEE Power and Energy Society General Meeting*. IEEE, San Diego, California, 1–8.

Liu, W. 2013. *Introduction to Hybrid Vehicle System Modeling and Control*. Wiley, Hoboken, New Jersey.

Lukic, S.M., J. Cao, R.C. Bansal, F. Rodriguez, A. Emadi. 2008. Energy storage systems for automotive applications. *IEEE Transactions on Industrial Electronics* **55**(6) 2258–2267.

Marra, F., G.Y. Yang, C. Traholt, E. Larsen, C.N. Rasmussen, S. You. 2012. Demand profile study of battery electric vehicle under different charging options. *2012 IEEE Power and Energy Society General Meeting*. IEEE, San Diego, California, 1–7.

MathWorks. 2015. Battery model implementation. URL `http://www.mathworks.com/help/physmod/sps/powersys/ref/battery.html`. Last accessed 20/7/2015.

Millner, A. 2010. Modeling lithium ion battery degradation in electric vehicles. *2010 IEEE Conference on Innovative Technologies for an Efficient and Reliable Electricity Supply (CITRES)*. IEEE, Waltham, Massachusetts, 349–356.

Moura, S.J. 2011. Techniques for battery health conscious power management via electrochemical modeling and optimal control. Ph.D thesis, University of Michigan, Ann Arbor, Michigan.

Moura, S.J., H.K. Fathy, D.S. Callaway, J.L. Stein. 2011. A stochastic optimal control approach for power management in plug-in hybrid electric vehicles. *IEEE Transactions on Control Systems Technology* **19**(3) 545–555.

Naberezhnykh, D., J J. Wardle, J J. Lowes, C. Herron, T. Brightman, T. Parker. 2012. Electric vehicle charging points for freight vehicles in central London (Version - Draft 0.7). Prepared for Central London FQP by Transport & Travel Research Ltd, in partnership with TRL and Zero Carbon Futures. URL `http://www.centrallondonfqp.org/app/download/12240926/CLFQP_EVCP_strategy+report_Final+v1+0.pdf`. Last accessed 9/6/2015.

Nesterova, N., H. Quak, S. Balm, I. Roche-Cerasi, T. Tretvik. 2013. Project FREVUE deliverable D1.3: State of the art of the electric freight vehicles implementation in city logistics. TNO and SINTEF. European Commission Seventh Framework Programme.

Nykvist, B., M. Nilsson. 2015. Rapidly falling costs of battery packs for electric vehicles. *Nature Climate Change* **5** 329–332.

Omar, N., M. Daowd, P. van den Bossche, O. Hegazy, J. Smekens, T. Coosemans, J. van Mierlo. 2012. Rechargeable energy storage systems for plug-in hybrid electric vehicles Assessment of electrical characteristics. *Energies* **5** 2952–2988.

Omar, N., P. van den Bossche, T. Coosemans, J. van Mierlo. 2013. Peukert revisited Critical appraisal and need for modification for lithium-ion batteries. *Energies* **6** 5625–5641.

Omar, N., M.A. Monem, Y. Firouz, J. Salminen, J. Smekens, O. Hegazy, H. Gaulous, G. Mulder, P. Van den Bossche, T. Coosemans, J. van Mierlo. 2014. Lithium iron phosphate based battery - Assessment of the aging parameters and development of cycle life model. *Applied Energy* **113** 1575–1585.

Ouyang, M., D. Ren, L. Lu, J. Li, X. Feng, X. Han, G. Liu. 2015. Overcharge-induced capacity fading analysis for large format lithium-ion batteries with LiyNi1/3Co1/3Mn1/3O2 + LiyMn2O4 composite cathode. *Journal of Power Sources* **279** 626–635.

Pelletier, S., O. Jabali, G. Laporte. 2015. Goods Distribution with Electric Vehicles: Review and Research Perspectives. *Transportation Science*, Forthcoming.

Peterson, S.B., J. Apt, J.F. Whitacre. 2010. Lithium-ion battery cell degradation resulting from realistic vehicle and vehicle-to-grid utilization. *Journal of Power Sources* **195** 2385–2392.

Preis, H., S. Frank, K. Nachtigall. 2014. Energy-optimized routing of electric vehicles in urban delivery systems. In: Helber, S., Breitner, M., Rösch, D., Schön, C. Graf von der Schulenburg, J-M., Sibbertsen, P., Steinbach, M., Weber, S., Wolter, A., eds. *Operations Research Proceedings 2012*. Springer International Publishing, Heidelberg, 583–588.

Psaraftis, H.N., ed. 2015. *Green Transportation in Logistics: The Quest for Win-Win Solutions*. International Series in Operations Research & Management Science, Vol. 226, Springer International Publishing, Heidelberg.

Sarasketa-Zabala, E., I. Gandiaga, L.M. Rodriguez-Martinez, I. Villarreal. 2014a. Calendar ageing analysis of a LiFePO4/graphite cell with dynamic model validations: Towards realistic lifetime predictions. *Journal of Power Sources* **272** 45–57.

Sarasketa-Zabala, E., I. Gandiaga, L.M. Rodriguez-Martinez, I. Villarreal. 2014b. Cycle ageing analysis of a LiFePO4/graphite cell with dynamic model validations: Towards realistic lifetime predictions. *Journal of Power Sources* **275** 573–587.

Sassi, O., W.R. Cherif-Khettaf, A. Oulamara. 2015. Vehicle routing problem with mixed fleet of conventional and heterogenous electric vehicles and time dependent charging costs. *International Journal of Mathematical, Computational, Statistical, Natural and Physical Engineering* **9**(3) 148–158.

Sauer, D.U. 2009. BATTERIES — ChargeDischarge Curves. In: Garche, J., Dyer, C., Moseley, P., Ogumi, Z., Rand, D., Scrosati, B. eds. *Encyclopedia of Electrochemical Power Sources*, Elsevier, Amsterdam, 443–451.

Schneider, M., A. Stenger, D. Goeke. 2014. The electric vehicle-routing problem with time windows and recharging stations. *Transportation Science* **48**(4) 500–520.

Shepherd, C.M. 1965. Design of primary and secondary cells II. An equation describing battery discharge. *Journal of the Electrochemical Society* **112**(7) 657–664.

Smith Electric Vehicles. 2015. Smith Newton United States spec sheet. URL http://www.smithelectric.com/wp-content/themes/barebones/pdfs/SmithNewtonUS_SpecSheet_2011.pdf. Last accessed 15/6/2015.

Stasko, T.H., H.O. Gao. 2012. Developing green fleet management strategies: Repair/retrofit/replacement decisions under environmental regulation. *Transportation Research Part A* **46** 1216–1226.

Sweda, T.M., I.S. Dolinskaya, D. Klabjan. 2014. Optimal recharging policies for electric vehicles. *Transportation Science*, forthcoming. URL http://users.iems.northwestern.edu/~dolira/tsiddk_evrecharging_rev.pdf. Last accessed 15/6/2015.

Taefi, T.T., J. Kreutzfeldt, T. Held, R. Konings, R. Kotter, S. Lilley, H. Baster, N. Green, M.S. Laugesen, S. Jacobsson, M. Borgqvist, C. Nyquist. 2015. Comparative analysis of European examples of freight electric vehicles schemes. In: Kotzab, H., Pannek, J., Thoben, K-D., eds. *Dynamics in Logistics – Proceedings of LDIC 2014*. Lecture Notes in Logistics, Springer, Berlin Heidelberg. Forthcoming.

Tan, L., L. Zhang, Q. Sun, M. Shen, Q. Qu, H. Zheng. 2013. Capacity loss induced by lithium deposition at graphite anode for LiFePO 4/graphite cell cycling at different temperatures. *Electrochimica Acta* **111** 802–808.

Tarascon, J.-M., M. Figliozzi. 2001. Issues and challenges facing rechargeable lithium batteries. *Nature* **414** 359–367.

Thackeray, M.M., C. Wolverton, E.D. Isaacs. 2012. Electrical energy storage for transportation – approaching the limits of, and going beyond, lithium-ion batteries. *Energy & Environmental Science* **5**(7) 7854–7863.

Tremblay, O., L.-A. Dessaint, A.-I. Dekkiche. 2007. A generic battery model for the dynamic simulation of hybrid electric vehicles. *2007 Vehicle Power and Propulsion Conference*. IEEE, Arlington, Texas, 284–289.

Tremblay, O., L.-A. Dessaint. 2009. Experimental validation of a battery dynamic model for EV applications. *International Battery, Hybrid and Fuel Cell Electric Vehicle Symposium (EVS24)*, Stavanger, Norway.

Trippe, A.E., R. Arunachala, T. Massier, A. Jossen, T. Hamacher. 2014. Charging optimization of battery electric vehicles including cycle battery aging. *2014 IEEE PES Innovative Smart Grid Technologies Europe (ISGT Europe)*. IEEE, Istanbul, Turkey, 1–6.

U.S. Department of Energy. 2012. Plug-in electric vehicle handbook for fleet managers. Office of Energy Efficiency and Renewable Energy, National Renewable Energy Laboratory (NREL). URL http://www.afdc.energy.gov/pdfs/pev_handbook.pdf. Last accessed 15/6/2015.

Vetter, J., P. Novák, M.R. Wagner, C. Veit, K.-C. Möller, J.O. Besenhard, M. Winter, M. Wohlfahrt-Mehrens, C. Vogler, A. Hammouche. 2005. Ageing mechanisms in lithium-ion batteries. *Journal of Power Sources* **147** 269–281.

Wang, J., P. Liu, J. Hicks-Garner, E. Sherman, S. Soukiazian, M. Verbrugge, H. Tataria, J. Musser, P. Finamore. 2011. Cycle-life model for graphite-LiFePO4 cells. *Journal of Power Sources* **196** 3942–3948.

Wenzl, H. 2009. BATTERIES — Capacity. In: Garche, J., Dyer, C., Moseley, P., Ogumi, Z., Rand, D., Scrosati, B. eds. *Encyclopedia of Electrochemical Power Sources*, Elsevier, Amsterdam, 395–400.

Wenzl, H., A. Haubrock, H.-P. Beck. 2013. Degradation of lithium ion batteries under complex conditions of use. *Zeitschrift fur Physikalische Chemie* **227**(1) 57–72.

Wohlfahrt-Mehrens, M., C. Vogler, J. Garche. 2004. Aging mechanisms of lithium cathode materials. *Journal of Power Sources* **127** 58–64.

Xu, B. 2013. Degradation-limiting optimization of battery energy storage systems operation. Master's thesis, ETH Zürich, Zürich, Switzerland.

Yong, J.Y., V.K. Ramachandaramurthy, K.M. Tan, N. Mithulananthan. 2015. A review on the state-of-the-art technologies of electric vehicle, its impacts and prospects. *Renewable and Sustainable Energy Reviews* **49** 365–385.

Zheng, H., L. Tan, L. Zhang, Q. Qu, Z. Wan, Y. Wang, M. Shen, H. Zheng. 2015a. Correlation between lithium deposition on graphite electrode and the capacity loss for LiFePO4/graphite cells. *Electrochimica Acta* **173** 323–330.

Zheng, Y. Y.-B. He, K. Qian, B. Li, X. Wang, J. Li, S.W. Chiang, C. Miao, F. Kang, J. Zhang. 2015b. Deterioration of lithium iron phosphate/graphite power batteries under high-rate discharge cycling. *Electrochimica Acta* **176** 270–279.

Zheng, Y. Y.-B. He, K. Qian, B. Li, X. Wang, J. Li, C. Miao, F. Kang. 2015c. Effects of state of charge on the degradation of LiFePO4/graphite batteries during accelerated storage test. *Journal of Alloys and Compounds* **639** 406–414.

Zündorf, T. 2014. Electric vehicle routing with realistic recharging models. Master's thesis, Karlsruhe Institute of Technology, Karlsruhe, Germany.